Influence of Ground Motion Type on Nonlinear Seismic Behaviour and Fragility of Corrosion-Damaged Reinforced Concrete Bridge Piers

Ebrahim Afsar Dizaj[a*], Mohammad M Kashani[b]

[a]Assistant Professor, Department of Civil Engineering, Azarbaijan Shahid Madani University, Tabriz, Iran. (corresponding author), Email: ebrahim.afsardizaj@azaruniv.ac.ir

Address: Iran, Tabriz, Azarbaijan Shahid Madani University, Faculty of Engineering, Department of Civil Engineering

Phone number: +989141581825

ORCID: https://orcid.org/0000-0002-7755-9983

[b]Associate Professor, Faculty of Engineering and Physical Sciences, University of Southampton, Southampton, SO17 1BJ, United Kingdom, Email: mehdi.kashani@soton.ac.uk

ORCID: https://orcid.org/0000-0003-0008-0007

Influence of Ground Motion Type on Nonlinear Seismic Behaviour and Fragility of Corrosion-Damaged Reinforced Concrete Bridge Piers

Ebrahim Afsar Dizaj[1*], Mohammad M Kashani[2]

[1]Assistant Professor, Department of Civil Engineering, Azarbaijan Shahid Madani University, Tabriz, Iran. (corresponding author), Email: ebrahim.afsardizaj@azaruniv.ac.ir

[2]Associate Professor, Faculty of Engineering and Physical Sciences, University of Southampton, Southampton, SO17 1BJ, United Kingdom, Email: mehdi.kashani@soton.ac.uk

Abstract

Two identical reinforced concrete (RC) bridge piers including a rectangular and a circular section are considered. The influence of corrosion damage, non-stationary characteristics of ground motions, and cross-sectional shape on nonlinear dynamic behaviour, failure mechanism and failure probability of these piers is investigated. An advanced modelling technique, capable of modelling coupled influence of inelastic buckling and low-cycle fatigue degradation of reinforcement, is employed to simulate the nonlinear structural behaviour of the piers. The considered bridge piers with various mass loss ratios (as a measure of corrosion) are subjected to a series of static pushover analyses and incremental dynamic analyses under three different suites of ground motions such as, Far-Field (FF), Near-Field With Pulse (NFWP), and Near-Field with No Pulse (NFNP). Furthermore, an advanced matching algorithm is used to investigate the effect of non-stationary content of near-field earthquake records including the presence of large pulses in ground motion time series on the nonlinear dynamic behaviour of the corrosion-damaged RC bridge piers. Finally, fragility curves are developed for each corroded bridge pier with different corrosion ratios subjected to each ground motion suite. Analyses results show that the failure mechanism of the corrosion damaged bridge piers significantly depends on the cross-sectional shape and ground motion type. It is concluded that while both of the piers with slight corrosion levels are much more vulnerable under NFWP ground motions than those under FF and NFNP ground motions; the

probability of failure of the extremely corroded bridge piers is approximately the same regardless of ground motion type.

Keywords: corrosion; incremental dynamic analysis; seismic fragility, failure mechanism; ground motion type; low-cycle fatigue

1. Introduction

Over the past couple of decades, structural vulnerability and seismic fragility analysis of deteriorated reinforced concrete (RC) structures have received significant attention around the world (ASCE 2013; Ghosh and Sood 2016; Dizaj *et al*. 2018a; Choe *et al*. 2008, 2009; Titi *et al*. 2014; Li *et al*. 2015; Alipour *et al*. 2011; Yuan *et al*. 2017; Yalciner *et al*. 2012; Sun *et al*. 2020; Xu *et al*., 2020). Amongst the several deteriorating mechanisms of RC structures, the chloride-induced corrosion of reinforcing bars is recognised as the most destructive mechanism. It has raised significant concern in countries near coastlines (Gaal 2004; Wallbank 1989). Considering the large number of corrosion-damaged structures located in high seismicity regions, the antagonistic influence of corrosion phenomenon on ductility and strength of such structures, coupled with dynamic earthquake loading may lead to early and undesirable failure mechanisms (Ghosh and Padgett 2010; Camnasio 2013; Biondini *et al*. 2015).

Numerous experimental and numerical studies have been carried out on corrosion damaged RC components (Kashani *et al*. 2019a; Meda *et al*. 2016; Imperatore 2017; Rajput *et al*. 2019; Ge *et al*., 2020; Vecchi and Belletti 2021). Moreover, an extensive number of studies have been devoted to evaluating the seismic reliability of corroded RC components/structures (Rao *et al*. 2017; Guo *et al*. 2015; Biondini and Frangopol 2009; Gu *et al*. 2018; Faroz *et al*. 2016; Zhang *et al*., 2019; Bagheri *et al*., 2020; Firouzi *et al*., 2020). The conclusion of these studies approves that corrosion of reinforcement increases the likelihood of catastrophic collapse in RC structures. However, the effects of corrosion on seismic damage limit states (DLSs) have not been extensively investigated. More recently, the findings

of the study conducted by Dizaj *et al*. (2018a), demonstrated that the time-invariant DLSs are not appropriate measures to assess the seismic fragility of corrosion damaged RC structures, since they underestimate the probability of failure of corroded structures.

Seismic performance of corroded RC structures under real earthquake ground motion records has been recently investigated in several studies (Dizaj *et al*. 2018a; Guo *et al*. 2015; Ni Choine *et al*. 2016; Cui *et al*. 2018; Deng *et al*. 2018; Billah and Alam 2018). Dizaj *et al*. (2018a) employed 22 pairs of far-field ground motion record set, according to the recommendation of FEMA P695 (2009), to study the nonlinear dynamic response of corrosion damaged RC frames. Ni Choine *et al*. (2016) studied the nonlinear dynamic behaviour of integral bridges using a set of 100 ground motions with a wide range of magnitude from 4.7 to 6.5 M_w. Cui *et al*. (2018) evaluated the structural vulnerability of reinforced concrete bridge substructures in aggressive environments using a suite of fifty ground motions varied in magnitude (5.7 to 7.2 M_w).

The impact of non-stationary characteristics of ground motion records on the nonlinear dynamic response, failure mechanism and seismic fragility of corroded RC structures, however, have not been studied in any of the above-mentioned studies. The previous studies on uncorroded RC structures (Lu *et al*. 2018) showed that the nature of earthquake excitation has a pronounced effect on failure mechanisms and the nonlinear dynamic behaviour of such structures. For instance, the far-field ground motions gradually increase the energy within the structure; while pulse-like near-field ground motions expose the structure in a remarkably severe demand in a short time at the beginning of the earthquake shaking (Lu *et al*. 2018). Moreover, according to the study conducted by Pu *et al*. (2018), near-field ground motions are expected to cause a higher acceleration response in structures in comparison with far-field ground motions with the same magnitude. This shows that the nature of ground motion records plays a critical role in the seismic fragility analysis of RC structures. Therefore, there is a vital need for a rigorous study

to investigate the influence of ground motion type on the seismic failure and fragility of corroded RC structures.

RC bridge piers are normally constructed in rectangular and circular cross-sectional shapes. The differences in geometry and arrangement of reinforcing bars between these two cross-sections result in a different distribution of stresses and strains in the plane of bending when the column is subjected to flexural loading. For instance, the outmost reinforcing bar in a tension side of the circular columns sustains the largest tensile strain and stress in the section, while the largest tensile strain and stress in an equivalent rectangular section are distributed among a number of reinforcing bars on the tension face. This could result in fracture of the reinforcement in tension and severe low-cycle fatigue damage under cyclic loading. Furthermore, the compressive failure of concrete in circular columns under uni-directional loading is more gradual in comparison with rectangular columns. A recent study by Dizaj *et al*. (2018b) demonstrated that corrosion of reinforcing bars changes the failure modes and seismic DLSs of the RC columns. Therefore, corrosion-induced damage coupled with cross-sectional shape may result in various modes of failure in RC columns.

1.1 Research Novelty and Contribution

While several studies have been dedicated to investigating the structural vulnerability of corrosion-damaged RC members, there is a significant paucity in the literature to investigate the influence of corrosion damage together with the influence of ground motion types and cross-sectional shape on seismic fragility of ageing RC bridge piers. In previous studies (Dizaj et al., 2018a, 2018b; Kashani et al., 2015b, 2016), the authors of this paper developed advanced numerical techniques to model the nonlinear behaviour of the corroded and uncorroded RC columns. These advanced numerical models paved the way to investigate the multiple failure modes of corroded RC columns with different cross-sectional shapes under different earthquake scenarios. Therefore, the novel contributions of the research

presented in this paper are: (*i*) investigation of the effects of corrosion damage together with ground motion types, and cross-sectional shapes on failure modes and seismic fragility of ageing RC bridge piers; and (*ii*) investigation of the impact of large earthquake pulses in near-field ground motions, on the nonlinear dynamic response, and seismic fragility of corroded RC bridge piers with different cross-section geometries and corrosion damage. For the latter, an advanced algorithm is used for spectral matching (Alexander *et al,* 2014), which does not change the non-stationary characteristics of earthquake records and minimises the variation in the results due to variation in ground motion parameters.

Fig. 1 shows an overview of the methodology proposed in this study for failure analysis of deteriorated RC bridge piers. As Fig. 1 shows, the structural behaviour of two equivalent RC bridge piers such as, a rectangular and a circular column with different mass loss ratios (as a measure of corrosion) are modelled in OpenSees (McKenna 2011) using the advanced numerical modelling technique described in (Dizaj *et al*. 2018b; Kashani et al., 2016). The proposed bridge columns are analysed under three different suites of real earthquake ground motions such as: (*i*) Far-Field (FF), (*ii*) Near-Field With Pulse (NFWP), and (*iii*) Near- Field with No Pulse (NFNP), selected from FEMA P695 (2009). To track the structural behaviour of these columns from the elastic range all the way to complete failure, the selected ground motions are applied to the columns with a wide range of incrementally increasing intensities. Nonlinear dynamic responses of the proposed RC columns, as well as their failure mechanisms at the material scale with different ground motion types, mass loss ratios, and cross-sectional shapes, are compared. Moreover, based on the corrosion-dependent DLSs, the corrosion-dependent fragility curves for each ground motion type are developed. Results show that the failure mechanism, global nonlinear dynamic behaviour and failure probability of the proposed columns are significantly dependent on the ground motion type, corrosion degree and cross-sectional shape. For example, while under the NFWP set the failure mode of the uncorroded rectangular column is governed mainly by core concrete crushing; under the NFNP set, the low-cycle fatigue failure of reinforcing bars followed by core concrete crushing is its

dominant failure mode. Furthermore, based on the analyses results, the probability of failure of the considered circular columns with various mass loss ratios is generally higher than those of the corresponding rectangular columns under any type of ground motion.

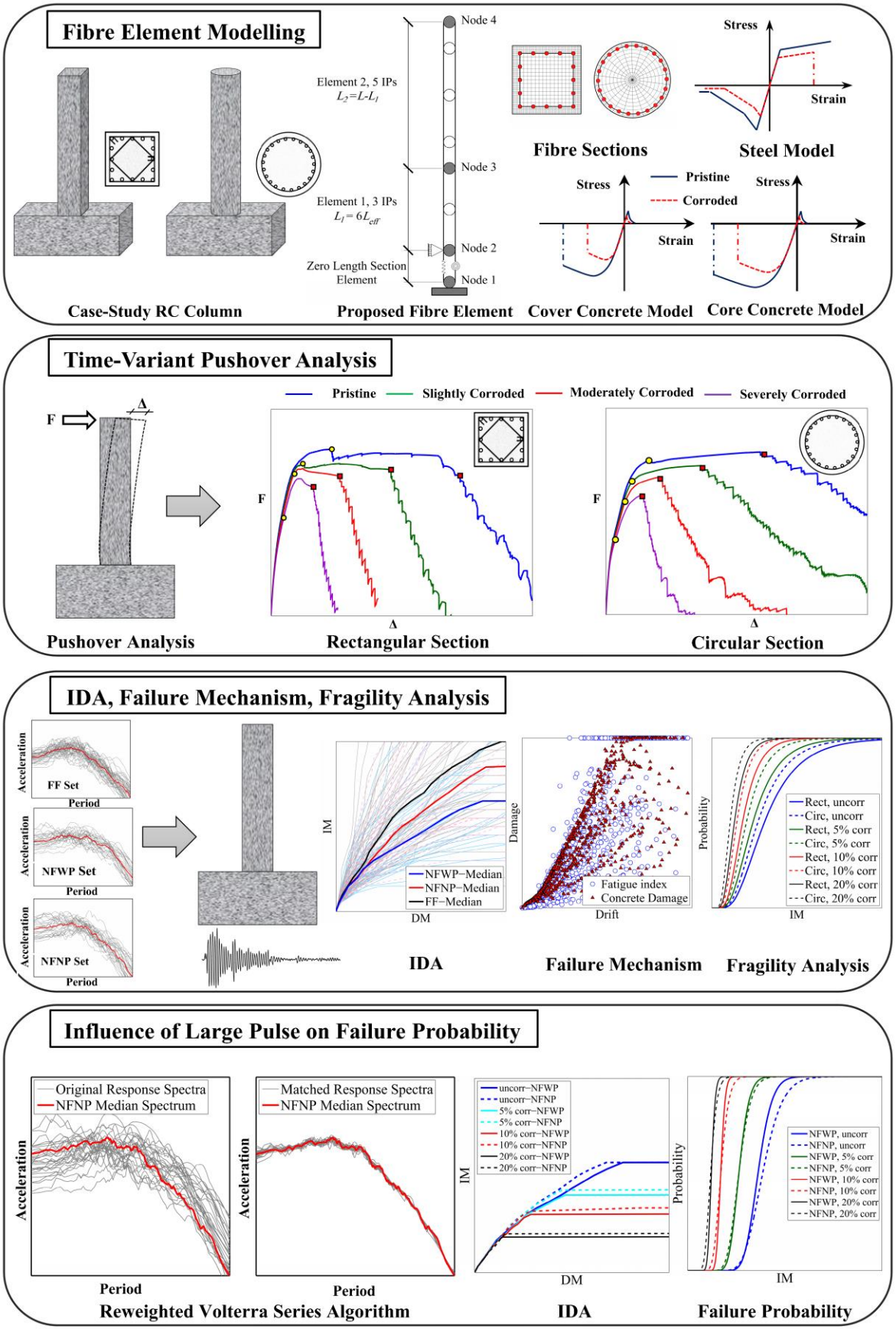

Fig. 1. An overview of the proposed methodology for failure analysis of deteriorated RC columns

2. Nonlinear Finite Element Model

2.1 Proposed RC Bridge Piers

In this study, two hypothetical RC bridge piers including a cantilever rectangular and a cantilever circular column are considered. To this end, first, the details and geometry of a circular RC column (Column 415) from experimentally tested columns by Lehman and Moehle (2000) are adopted here as a benchmark. Then, the rectangular column is designed to have the same properties as the circular column such as, height, longitudinal reinforcement ratio (ρ_l), ratio of effective buckling length of longitudinal reinforcement to its diameter (L_{eff} /d), fundamental period (T), volumetric ratio of transverse reinforcement (ρ_t) and axial force ratio ($N_u/(f_cA_g)$). The details of the proposed columns are shown in Fig. 2 and summarised in Table 1. In this table, A_g is the cross-sectional area of the columns.

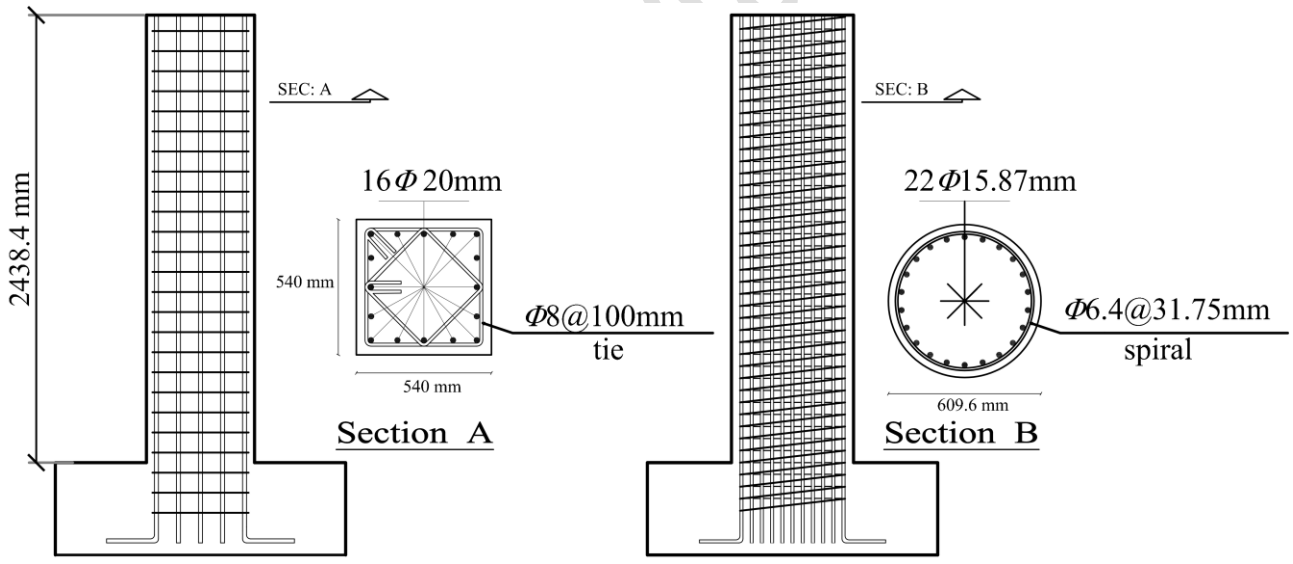

Fig. 2. The geometry and details of considered RC columns

Table 1. Details of the proposed columns

Column	L/D	L_{eff}/d	ρ_l	ρ_t	A_g (mm^2)	$N_u/(f_cA_g)$	T (sec)
Circular (Column 415) (Lehman *et al.*, 2004)	4	10	0.015	0.007	291715.5	0.07	0.25
Rectangular	4.5	10	0.017	0.008	291600	0.07	0.25

2.2 Proposed Finite Element Model

The structural behaviour of the proposed hypothetical RC columns is simulated in OpenSees (McKenna 2011) employing the nonlinear fibre beam-column element developed in Kashani *et al*. (2016) and Dizaj *et al*. (2018b). Using this modelling technique, the entire length of the column is discretised into several fibre sections at integration points. This methodology has been used to model the nonlinear cyclic response of corroded and uncorroded RC columns and has been validated successfully against experimental test results (Further details are available in (Dizaj *et al*. 2018b; Kashani *et al*. 2016; Salami 2016). The details of the implemented modelling technique are schematically shown in Fig. 3. As it is shown in Fig. 3, the proposed nonlinear fibre beam-column element consists of three elements: (*i*) a zero-length section element (available in the OpenSees) to account for the slippage of vertical reinforcement in the anchorage zone of the columns, (*ii*) a force-based element with 3 Integration Points (IPs), and length of 6 L_{eff} to address the strain localisation problem in its first integration point, and (*iii*) another element with 5 IPs. Here, L_{eff} is the effective buckling length of the longitudinal reinforcing bars which is calculated based on the procedure presented in (Dhakal and Maekawa 2002). The base of the column is assumed to be fully fixed, and the top of the column is considered to be free to move alongside the horizontal direction. Moreover, the P-delta secondary effects are modelled in the nonlinear analyses by using the P-Delta coordinate transformation option available in the OpenSees.

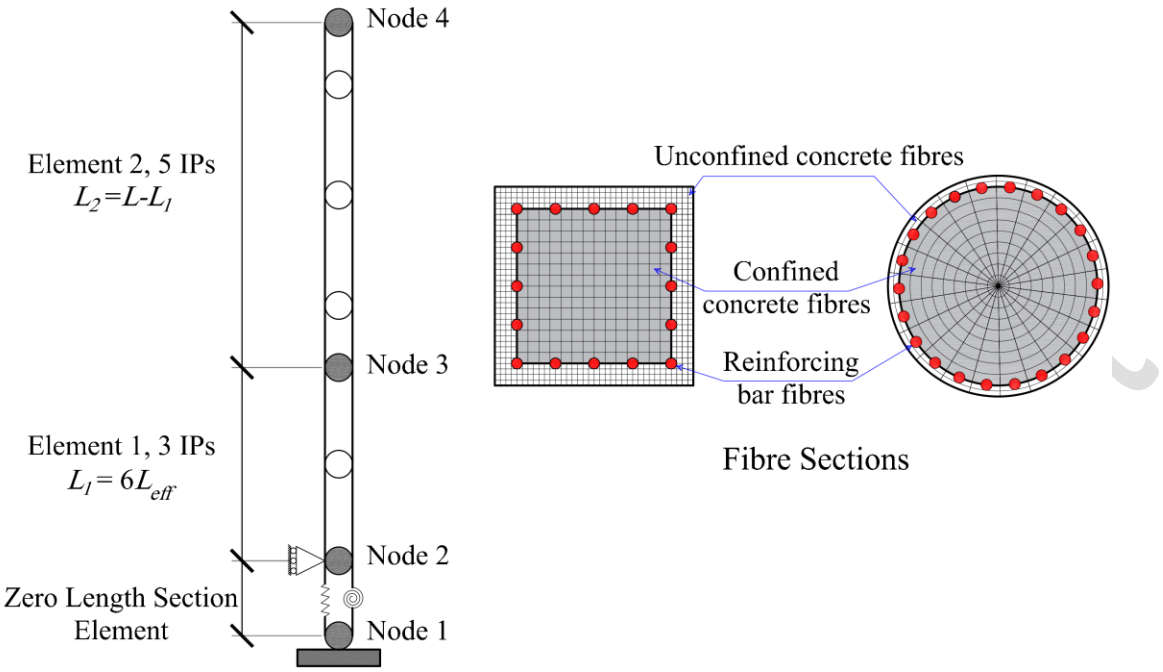

Fig. 3. The details of implemented fibre-based modelling technique

The key factor in the fibre element modelling technique is to correctly define the constitutive steel and concrete material models. In this study, the phenomenological hysteretic model developed by Kashani *et al*. (2015b) is employed to model the stress-strain law of reinforcing steel bars. This model is capable of capturing the adverse influence of corrosion damage on inelastic buckling and low cycle fatigue of corroded reinforcement. Fig. 4 compares the stress-strain behaviour of uncorroded reinforcing bars with that of 20% corroded reinforcements. Fig. 4 shows that the material model of reinforcing bars is capable of modelling the adverse influence of corrosion on ductility and strength of the reinforcements as well as its effect on their inelastic buckling behaviour.

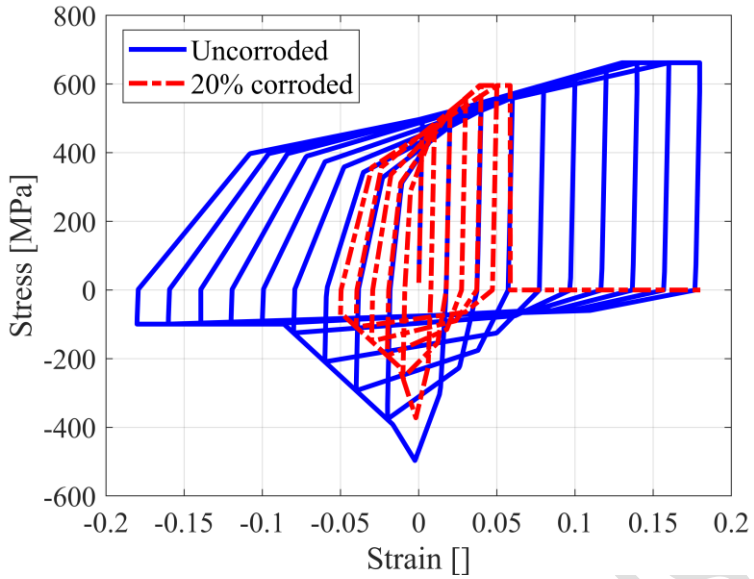

Fig. 4. The stress-strain behaviour of reinforcing bars

The stress-strain behaviour of confined and unconfined concrete in the circular section is modelled using the *Concrete04* uniaxial material model available in OpenSees. The compressive strength of the confined core concrete is modified using the model proposed by Mander *et al*. (1988). However, according to the study conducted by Kashani *et al*. (2018), the *Concrete04* is not appropriate to simulate the nonlinear response of rectangular columns, as it significantly overestimates the confinement level of rectangular/square cross-sections. Their parametric study showed that the modified Kent and Park model (Scott *et al*. 1982) works much better than Mander *et al*. (1988) model for rectangular and square cross-sections. Therefore, uniaxial material *Concrete02* is used instead. This model employs a parabolic curve in compression up to the peak compressive strength of the concrete, and a linear softening up to 20% of the peak strength. Using this model, the tensile behaviour of concrete is modelled through a bilinear curve. The modified Kent and Park model (Scott *et al*. 1982) is used to modifying the stress-strain relationship of the core concrete in rectangular section. For both the columns, corrosion-induced premature spalling of the concrete cover is modelled using the procedure proposed by Coronelli and Gambarrova (2004). Moreover, the adverse effect of corrosion on the nonlinear behaviour of core concrete is considered in numerical modelling through modifying the properties of transverse

reinforcement (further details are available in (Dizaj *et al*. 2018b). The ultimate compressive strain of confined core concrete is obtained using the following empirical equation proposed by Priestley and Paulay (1992):

$$\varepsilon_{cu,corr} = 0.004 + 1.4\left[\frac{\rho_{t,corr}\,\sigma_{yt,corr}\,\varepsilon_{ut,corr}}{\sigma_{cc,corr}}\right] \quad (1)$$

Where, $\sigma_{cc,corr}$ is the compressive strength of confined core concrete; $\sigma_{yt,corr}$, $\rho_{t,corr}$ and ε_{ut} are yield strength, volumetric ratio and tensile strain at maximum stress of corroded transverse reinforcements, respectively, according to Eqs. (2-4) (Du *et al*. 2018a, 2018b):

$$\frac{\sigma_{yt,corr}}{\sigma_{yt}} = 1 - 0.005\psi_t \quad (2)$$

$$\frac{\rho_{t,corr}}{\rho_t} = 1 - 0.01\psi_t \quad (3)$$

$$\frac{\varepsilon_{ut,corr}}{\varepsilon_{ut}} = 1 - 0.05\psi_t \quad (4)$$

where σ_{yt}, $\rho_{t,corr}$, ρ_t and ψ_t are yield strength, volumetric ratio, tensile strain at maximum stress and mass loss percentage of uncorroded transverse reinforcements, respectively. The ultimate compressive strain of unconfined concrete cover (corresponding to spalling) is assumed as 0.004 (Priestley and Paulay 1992).

Fig. 5 and Fig. 6 show the simulated compressive stress-strain response of the confined core concrete and unconfined concrete cover, respectively.

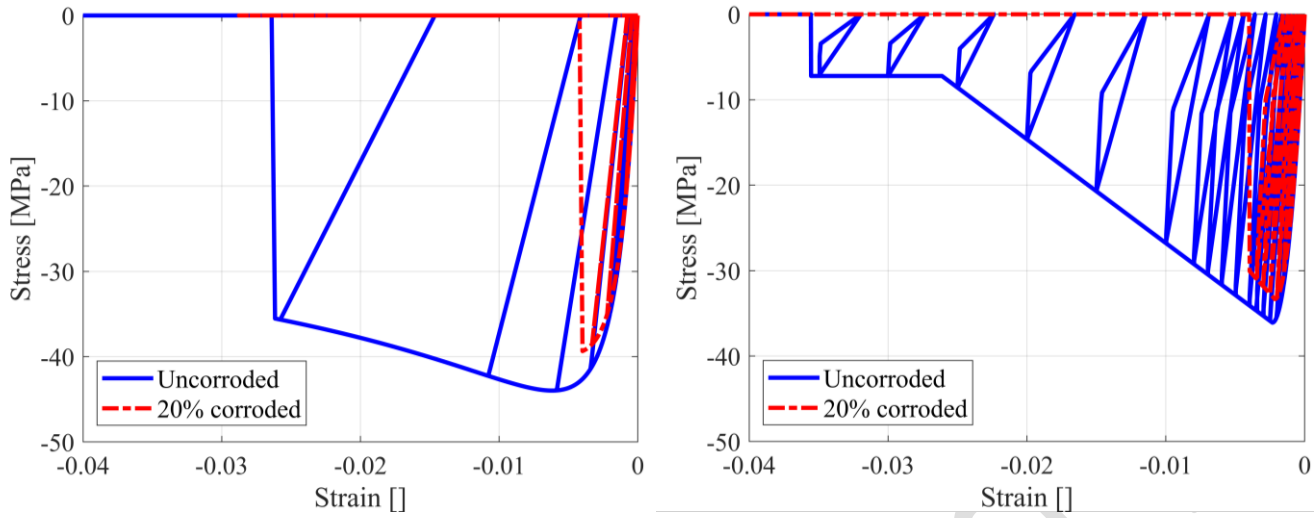

(b) **(b)**

Fig. 5. The compressive stress-strain behaviour of confined core concrete: (a) circular section; (b) rectangular section

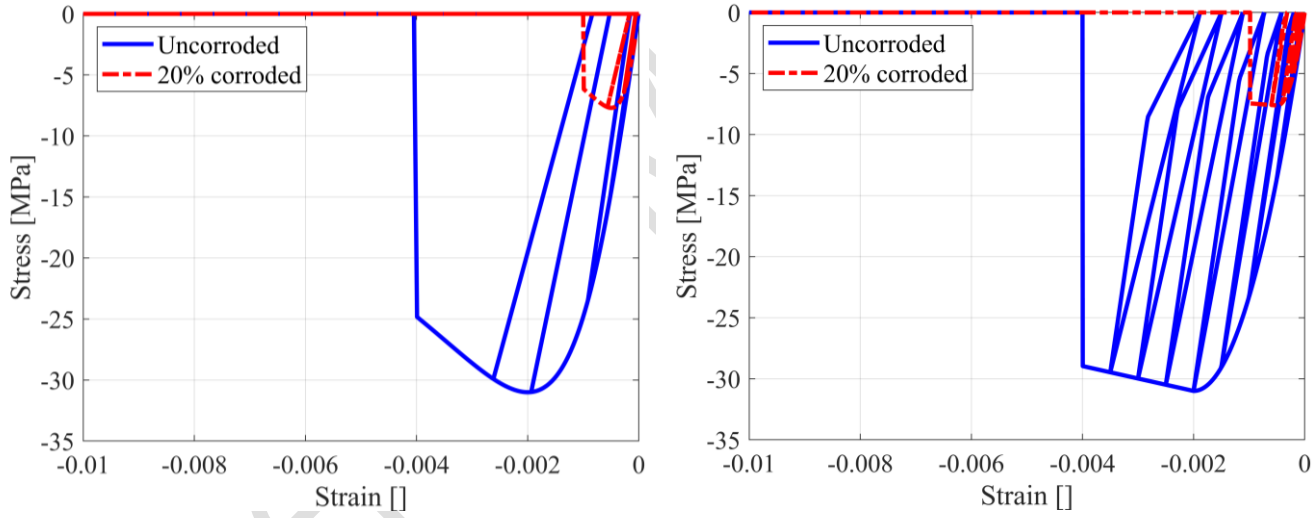

Fig. 6. The compressive stress-strain behaviour of unconfined concrete cover: (a) circular section; (b) rectangular section

To calculate the fatigue damage index of reinforcing bars the Coffin-Manson model (Manson 1965) is used, where the amplitude of plastic strain is calculated using Eq. (5):

$$\varepsilon_p = \Theta_f \left(2N_f\right)^{-\alpha} \tag{5}$$

where ε_p is the plastic strain amplitude, Θ_f and α are material constants and $2N_f$ is the number of half-cycles associated with the onset of fracture of steel reinforcement. In this study, Θ_f and α are considered

to be 0.192 and −0.602, respectively, according to the equations proposed by Kashani et al. (2015a). According to the results obtained by Kashani et al. (2015b), to account for the influence of corrosion on fatigue life of steel reinforcing bars α should be modified using the following equation:

$$\alpha_{corr} = \alpha\left[1+0.004\psi\right] \quad (6).$$

In Eq. (6) α_{corr} is material constant for corrosion-damaged steel reinforcements. In the OpenSees the uniaxial *Fatigue* model uses the Eq. (5) to calculate the accumulated fatigue damage in reinforcements. Therefore, in this study, the uniaxial *Fatigue* model is wrapped to the hysteretic buckling model to account for the LCF damage index. Using this material model, once the LCF damage index becomes equal to unity, the stress in the corresponding reinforcement drops to zero; i.e., the corresponding reinforcement is eliminated from the stiffness matrix of the structure.

Finally, for the zero-length section element, the stress-slip model of reinforcing bars proposed in (Zhao 2007), is adopted (further details are available in Dizaj *et al*. (2018a).

It is worth mentioning that the outcome of Dizaj et al. (2018b) indicated that the impact of uncertainties associated with structural properties and spatial variability of pitting corrosion is negligible if the pitting corrosion is modelled by modifying the yield and ultimate strength, ductility, inelastic buckling, low-cycle fatigue life, and cross-sectional area of reinforcements. Therefore, in the current study, an average area loss is considered; and then, the pitting corrosion effect is included in the material models. Further details on finite element modelling of corrosion damaged RC columns are available in Dizaj et al. (2018a).

3. Time-Variant Damage Limit States (DLSs)

Seismic fragility of uncorroded structures is generally evaluated using the time-independent seismic DLSs. However, previous studies by Dizaj *et al*. (2018a, 2018b) confirmed that the time-independent

DLSs are not sufficient for seismic performance assessment of corroded RC structures. Hence, the seismic DLSs of corroded structures should be defined as time-variant parameters; i.e. to be a function of corrosion damage.

To quantify the time-variant DLSs, monotonic pushover analyses carried out on the proposed columns with varied mass loss ratios such as, 0% (pristine column), 5%, 10% and 20%. It should be mentioned that due to the lack of reliable experimental data and validated empirical/analytical models in the literature to account for two-dimensional chloride penetration, for the sake of simplicity, it is assumed that all the reinforcements within the cross-section are subjected to one-dimensional ingress of chloride ions.

The pushover analyses results are shown in Fig. 7. It can be seen in Fig. 7 that increasing the mass loss results in a marked decline of capacity and ductility of the columns. To track the corrosion-damaged limit states, associated drifts of bar yielding, concrete cover spalling and core concrete crushing are mapped on the graphs. It should be noted that in any of the considered uncorroded and corroded columns the fracture of reinforcement did not take place. Dizaj *et al*. (2018a) reported that the associated drift of bar yielding, concrete cover spalling and core concrete crushing approximately coincide with those of moderate, extensive and complete collapse DLSs, respectively (as defined in HAZUS-MH MR5 (2010)). Fig. 7 shows that as mass loss increases columns fail in significantly lower drift ratios. For example, while the uncorroded circular column fails at an approximately 5% drift; its corresponding corroded column with 20% mass loss fails at about 1% drift (Fig. 7(b)).

The results shown in Fig. 7 and associated drift ratios of each DLS are used in section 5 of this paper to develop time-variant fragility curves.

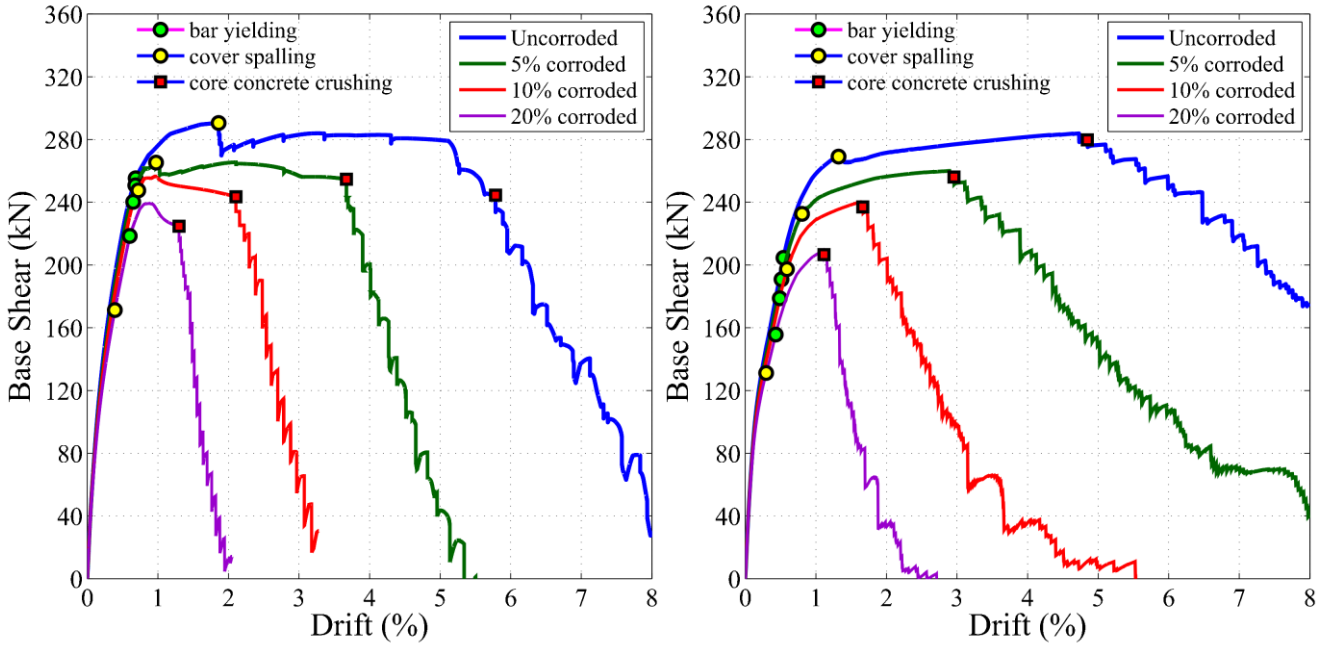

(a) **(b)**

Fig. 7. Results of pushover analysis: (a) rectangular column; (b) circular column

4. Incremental Dynamic Analysis (IDA)

4.1 Selection of Ground Motions

To study the effects of ground motion type on seismic fragility of corrosion-damaged columns, three different types of ground motions suggested in FEMA P695 (2009) are used. The selected suites of ground motions include: (*i*) Far-Field (FF), (*ii*) Near-Field With Pulse (NFWP), and (*iii*) Near-Field with No Pulse (NFNP). The suite of FF records includes 44 individual records (22 pairs) with varied PGA from 0.21g to 0.82g, the suite of NFWP records includes 28 individual components (14 pairs) with varied PGA from 0.22g to 0.87g, and the suite of NFNP records includes 28 individual components (14 pairs) with varied PGA from 0.28g to 1.43g. The details of selected ground motion record sets are provided in FEMA P695 (2009). Spectral acceleration response of the selected ground motion suites as well as their median spectra are shown in Fig. 8. Moreover, the fundamental period of the studied uncorroded columns

is shown in Fig. 8 by a vertical solid line. It should be noted that the fundamental periods of the corroded columns are very close to those of uncorroded columns. For example, the calculated value of T_1 for the uncorroded, 5% corroded, 10% corroded and 20% corroded rectangular RC columns are 0.257 sec, 0.259 sec, 0.261 sec, and 0.264 sec, respectively. This is because, the calculated period is based on the uncracked elastic section; and hence, corrosion of reinforcing bars has a negligible influence on the natural period of such columns. Moreover, the outcome of a shaking table study carried out in (Kashani et al., 2019b) shows that comparing to concrete cracking/spalling, damage in steel reinforcement has almost no impact on the fundamental period of RC structures. Fig. 8 shows that the corresponding acceleration response of the fundamental period of the columns is approximately ranged from 0.25g to 1.75g for the NFWP suite (Fig. 8(a)); 0.3g to 3.25g for the NFNP suite (Fig. 8(b)), and 0.3g to 1.9g for FF suite (Fig. 8(c)).

The intensity measure of an input ground motion record can be described in terms of simple metrics such as PGA, PGV, PGD, .etc. However, these quantities are correlated only with the ground motion characteristics and are not connected with the response of the structure studied. Therefore, to conduct the IDAs (Vamvatsikos and Cornell, 2002), herein Sa(T_1) is selected as the intensity measure because it contains information on the dynamic characteristics of the considered RC columns. Moreover, this measure enables considering the slight change in the fundamental period of the considered columns due to the corrosion of reinforcements. To this end, firstly, the spectral acceleration of each selected ground motion record is normalised to the spectral acceleration at the fundamental period of each column (Sa (T_1)). Secondly, through applying incremental scale factors on each ground motion a series of time-history analyses carried out on the columns. The applied scale factors to run IDAs of uncorroded and 5% corroded columns ranged from 0.1g to 4g with 0.1g intervals, and for the 10% and 20% corroded columns ranged from 0.1g to 3g with the same intervals. To build a single IDA curve in each time-history analysis, the maximum value of the drift ratio is calculated and plotted against its corresponding scale factor.

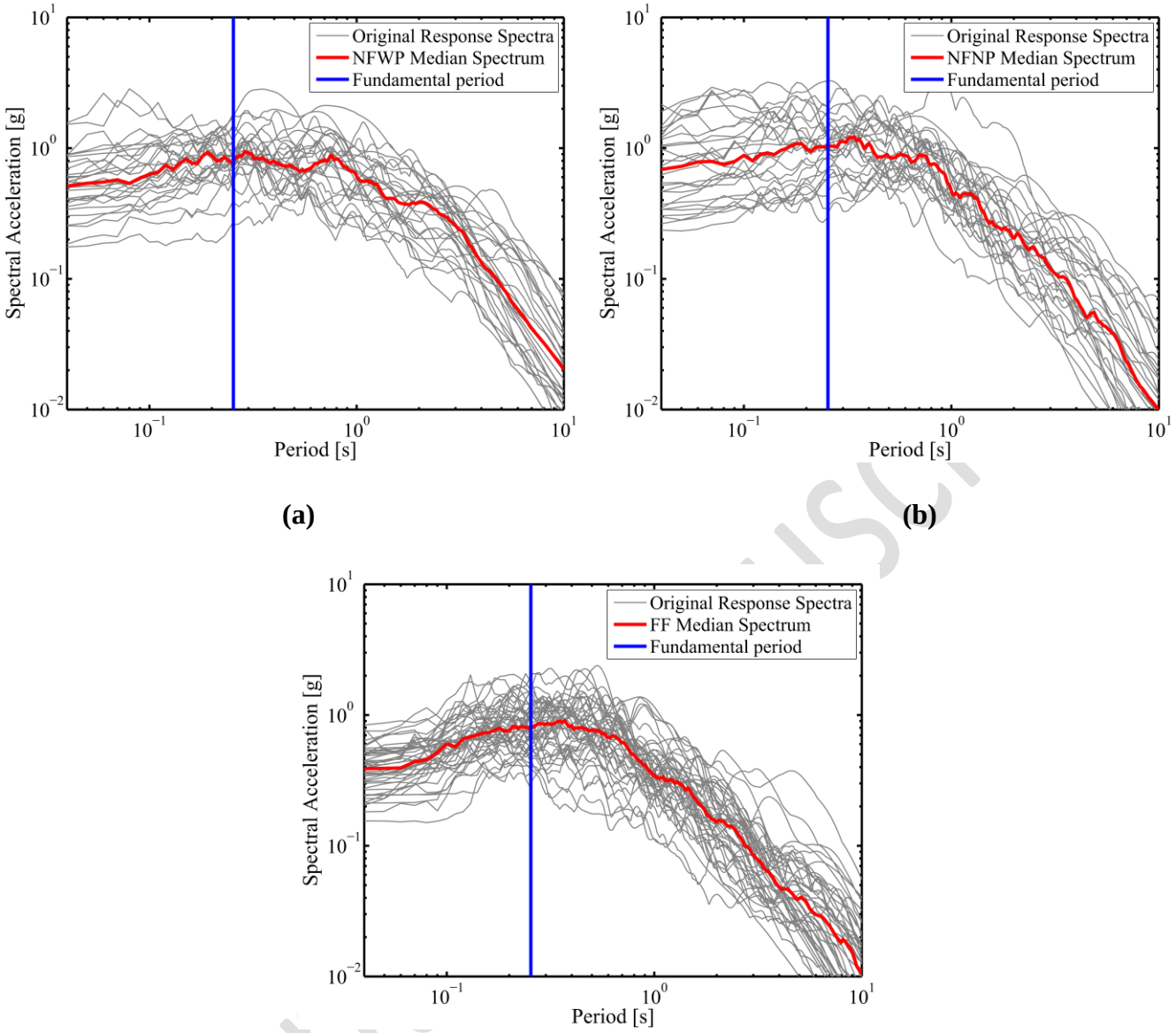

Fig. 8. Spectral acceleration response of the selected ground motions suites: (a) NFWP; (b) NFNP; (c) FF

4.2 Discussion of IDA results

4.2.1 Global Dynamic Behaviour

Fig. 9 shows the IDA results of the rectangular column for different mass loss ratios and ground motion types. The median IDA curves are also plotted in each case to summarise the IDA results of each suite

of ground motions. Moreover, the drift ratio corresponding to complete collapse DLS of each column with different corrosion levels is extracted from Fig. 7, and plotted in Fig. 9 by a vertical solid line.

Fig. 9 shows that for all the considered mass loss ratios the median IDA curve of FF ground motions is on top, and the NFWP is below the other two median curves. This might be due to the influence of ground motion duration and intensity; where, FF ground motions gradually increase the damage in both the uncorroded and corrosion damaged rectangular columns, and hence, under FF ground motions their spectral acceleration response is much higher than the near-field suites. This finding contradicts the statement given by Pu *et al*. (2018). The near-field ground motions, however, result in impulsive damage (at the beginning) on the columns, and hence, the column cannot respond to the ground motion after that. This can be seen in Fig. 9(a), where most of the NFWP ground motions have been pushed to the nonlinear region quickly (after a large pulse); and therefore, they have not experienced higher accelerations after that. Moreover, based on Fig. 8(a), the response spectrum of the NFWP ground motions has maximum responses at periods away from the natural period of the columns; and therefore, the acceleration response of the structures depends on the non-stationary frequency content of the ground motions. For example, while the maximum spectral acceleration response of 5% corroded rectangular column subjected to FF ground motions is approximately 2.5g; for the same column under NFWP ground motions, it is around 1.5g (Fig. 9(b)). Moreover, the median IDA results shown in Figs. 9 (a) and 9(b) show that for a given intensity level of the ground motion record, the uncorroded and slightly corroded rectangular columns, experience higher drift ratios under near field ground motions (NFWP and NFNP set). For example, as Fig. 9(a) shows, while for $Sa(T_1)$=2g the median drift ratio of the uncorroded rectangular column is approximately 0.07 and 0.043 under NFWP and NFNP ground motions, respectively; its drift ratio is at the vicinity of 0.035 when it is subjected to FF ground motion suite. However, for higher mass loss ratios, the median response of the rectangular column becomes plateau at approximately the same drift ratio under all ground motion types, and the median IDA curves become much closer to each other. For

instance, as Fig. 9(d) shows, for 20% mass loss there is no significant difference between the median responses of the column under FF and NFNP ground motions. This is because, as corrosion damage increases, columns have brittle failure points, and therefore, they all fail at approximately a similar intensity of ground motion records regardless of ground motion type.

The results presented in Fig. 9 are separately plotted for each ground motion suite and corrosion degree, and are available in Fig. S1, Fig. S3 and Fig. S5 of the attached "Supplementary Figures" file.

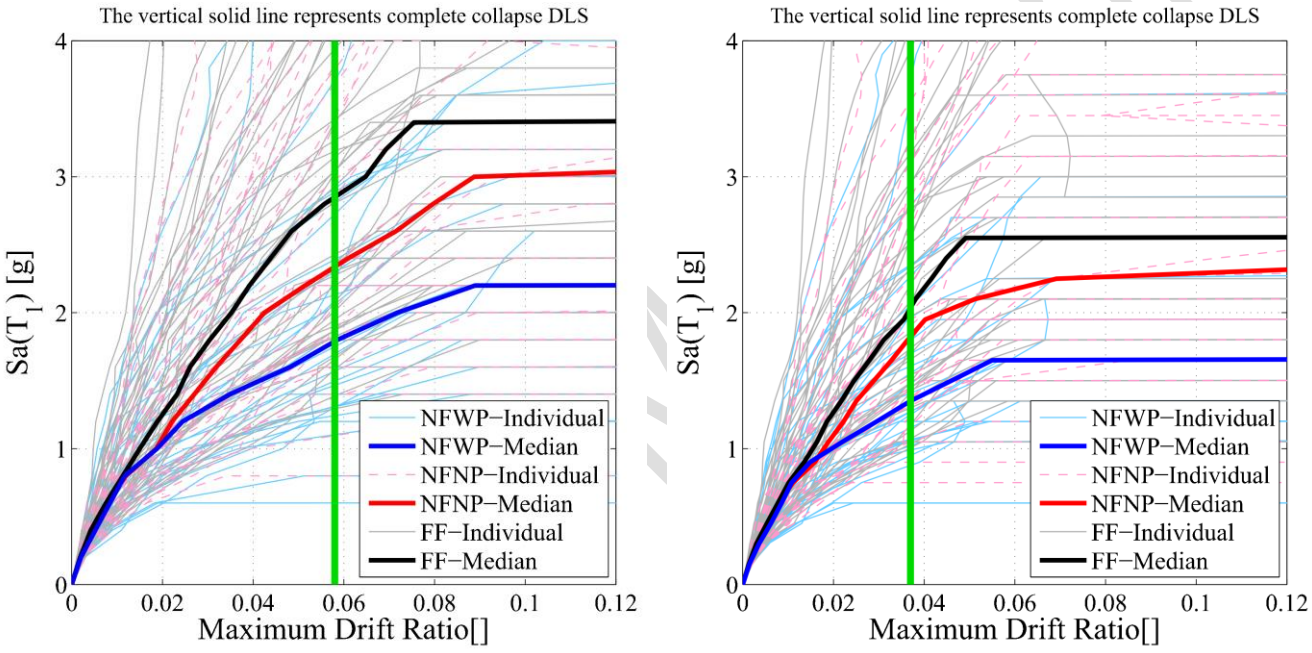

(a) **(b)**

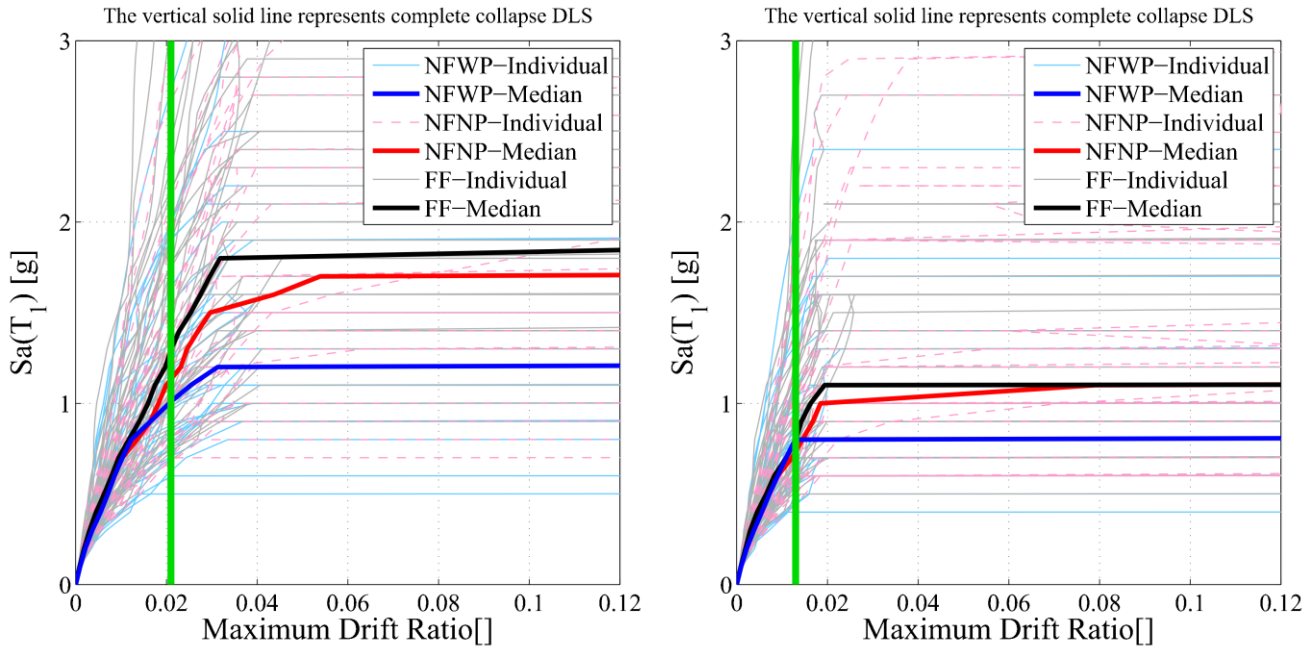

(c) **(d)**

Fig. 9. Results of IDA for rectangular column: (a) uncorroded; (b) 5% corroded; (c) 10% corroded and (d) 20% corroded

Fig. 10 presents the IDA results of the circular column. Comparing to Fig. 9, there is a similar trend between median IDA curves of FF, NFWP and NFNP ground motions. In all the cases, the median IDA curve of FF ground motions is superior to other types. However, the median IDA response of the circular column becomes plateau at higher drift ratios and higher earthquake intensity levels (higher $Sa(T_1)$ values) under FF ground motions in comparison to NFWP and NFNP ground motions. For example, while the median response of uncorroded circular column subjected to FF ground motions becomes plateau at approximately 0.12 drift ratio; it takes place at approximately 0.105 drift ratio under NFNP ground motions. Moreover, for the severely corroded circular column (Fig. 10(d)), the intensity measure of earthquake records corresponding to the failure point is almost the same for all ground motion types.

The results given in Fig. 10 are separately plotted and are provided in Fig. S2, Fig. S4 and Fig. S6 of the attached "Supplementary Figures" file.

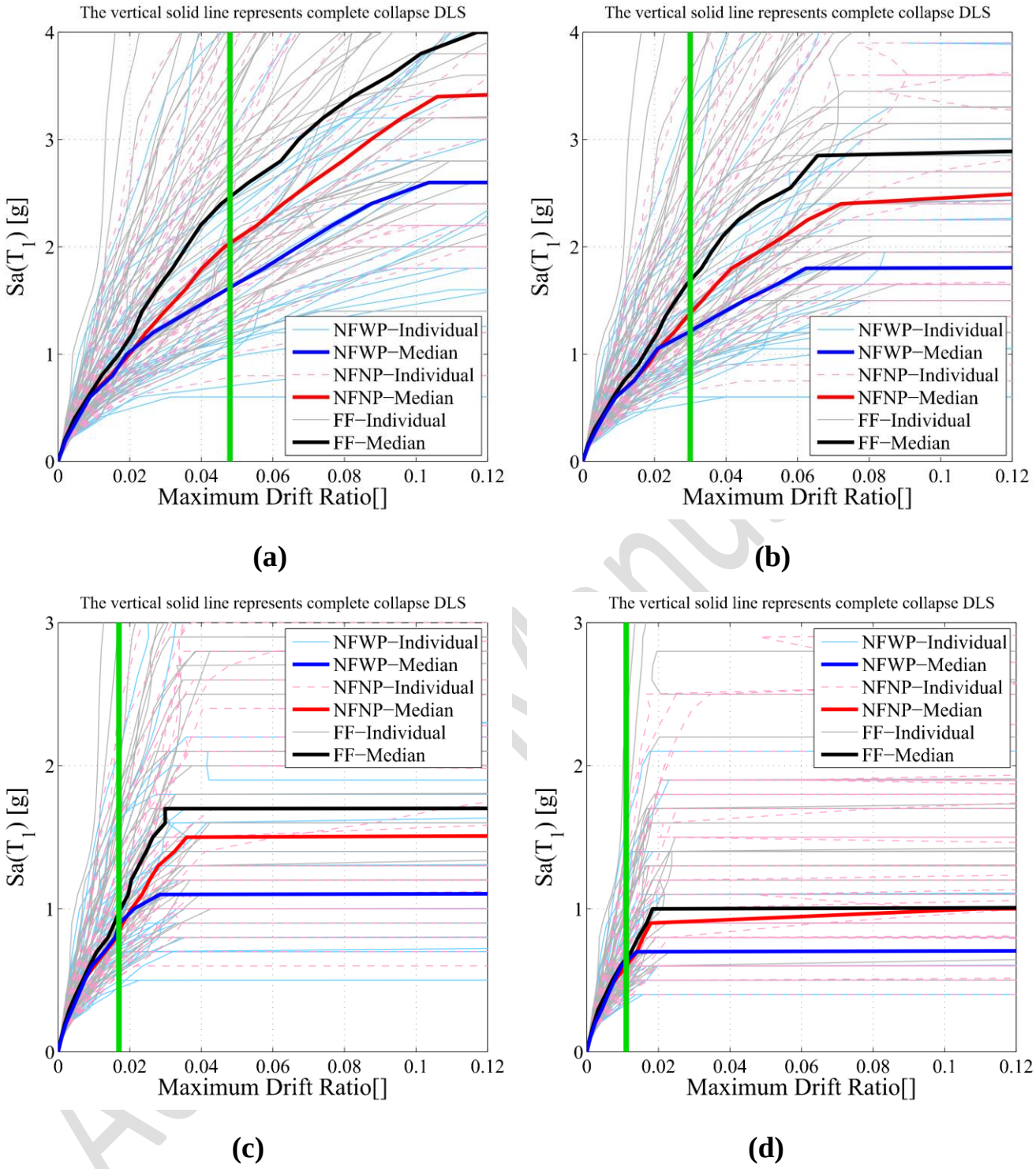

Fig. 10. Results of IDA for circular column: (a) uncorroded; (b) 5% corroded; (c) 10% corroded and (d) 20% corroded

To investigate the impact of cross-sectional shape and corrosion damage on seismic behaviour of proposed RC columns (Fig. 11), the median IDA curves of the rectangular column under each suite of ground motions are compared with those of the circular column. Fig. 11 shows that for lower mass losses

(i.e. uncorroded and 5% corroded), the spectral acceleration response of the circular column is higher than the rectangular column. This might be due to the gradual failure of the uncorroded and lightly corroded circular columns. However, the median IDA curves of both the rectangular and circular columns with 10% and 20% of mass loss become plateau at about the same input earthquake intensity level. Moreover, the reason for different trends in median IDA responses of uncorroded and slightly corroded rectangular and circular columns can be attributed to the different cross-section geometry and distribution of reinforcing bars within these two cross-sections. In circular columns, the compressive failure of concrete under uniaxial loading is more gradual in comparison to the rectangular columns. This is because in the compression face of a circular column the outmost single bar gets overloaded and buckles, which results in the initiation of core concrete crushing gradually. Then it is followed by the progressive buckling of other bars and more concrete crushing. However, in a rectangular column, this phenomenon happens at a later stage but when it happens, all the bars in one face (compression face) buckle together. Furthermore, while in the rectangular column the tensile stress in the outmost tension side of the section is tolerated by a number of reinforcements; in the circular column, the largest tensile stress and strain in the tension face of the section is tolerated by a reinforcing bar. This will result in different failure modes in the circular and rectangular sections. The failure mechanisms of the considered columns are further discussed in section 4.2.2.

However, when columns are heavily corroded, the failure of both the columns under unidirectional loading is very brittle (almost identical).

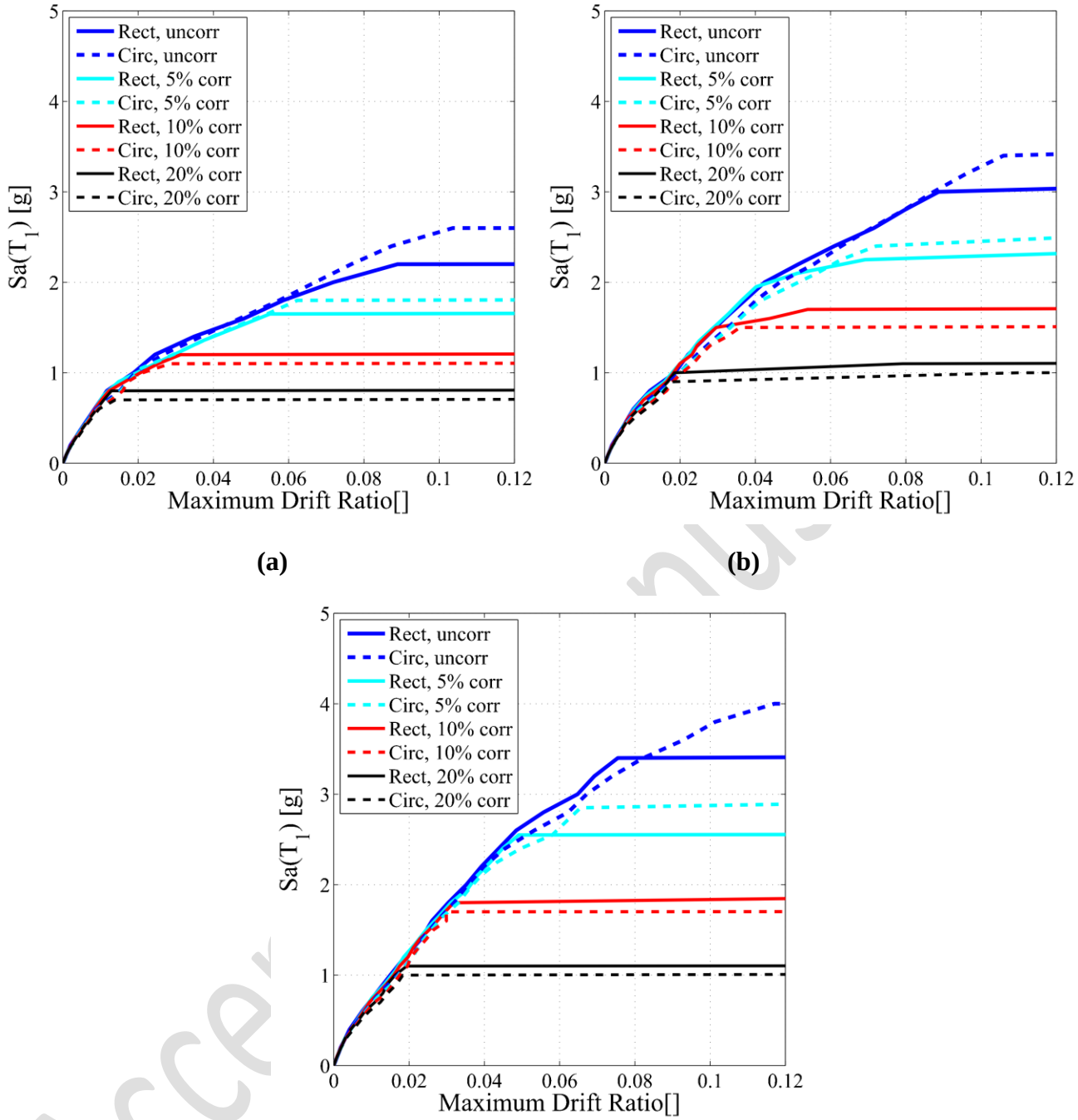

Fig. 11. Median IDA curves: (a) NFWP set; (b) NFNP set and (c) FF set

Fig. 12 shows the influence of ground motion type and cross-sectional shape for a given corrosion degree on median IDA response of the considered RC columns. As Fig. 12(a) shows, for each ground motion suite, the uncorroded circular column fails at higher spectral accelerations comparing to the rectangular

column. However, for 10 percent of mass loss, the median IDA response of both the columns become approximately the same under a specific ground motion suite (Fig. 12(c)). Furthermore, severely corroded columns show approximately similar nonlinear dynamic behaviour regardless of cross-section geometry and ground motion type (Fig. 12(d)).

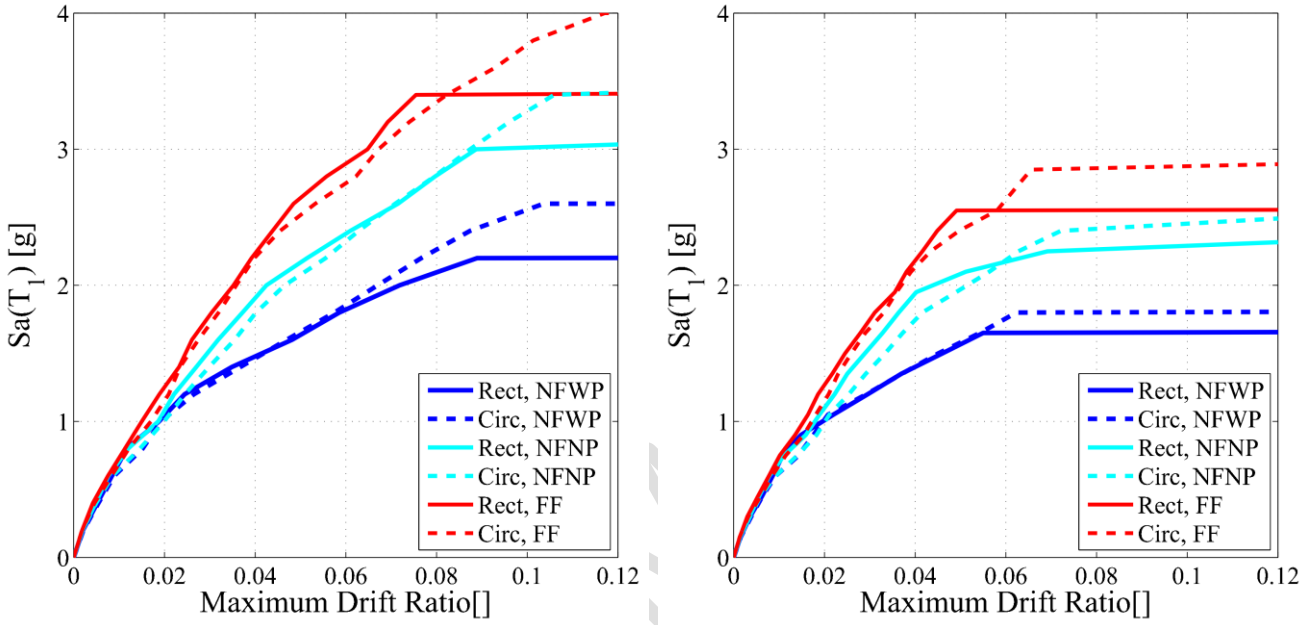

(a) **(b)**

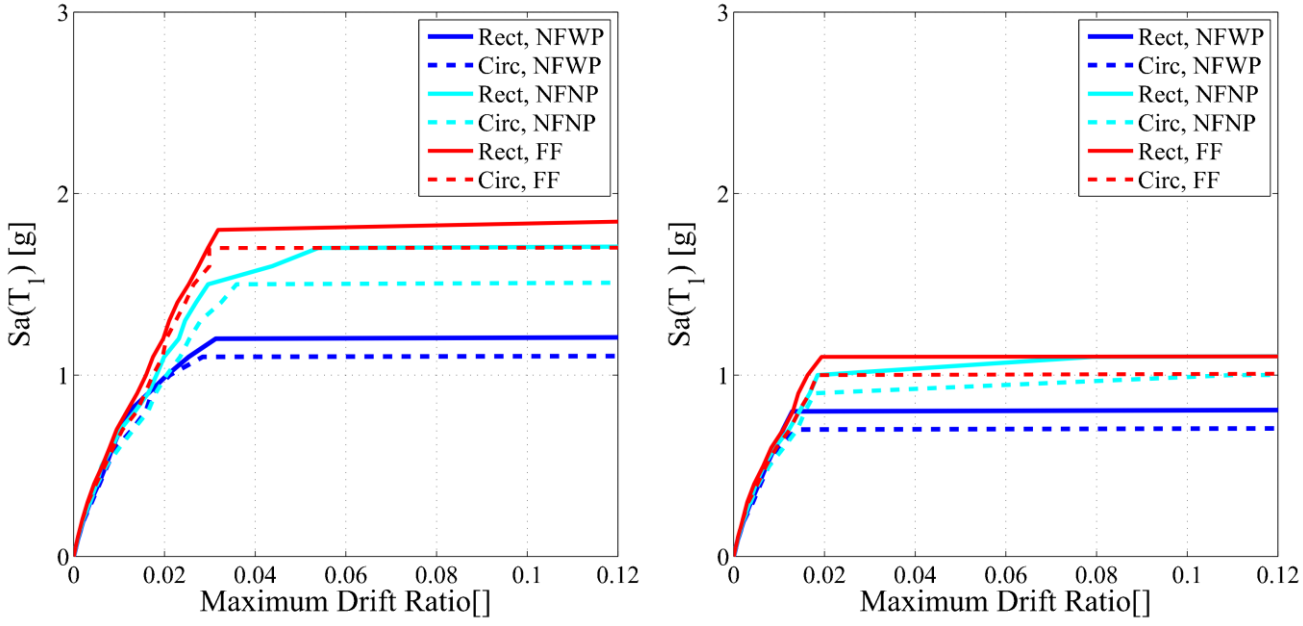

(c) **(d)**

Fig. 12. Median IDA curves for various degrees of corrosion: (a) ψ=0 %; (b) ψ=5 %; (c) ψ=10 % and (d) ψ=20 %

4.2.2 Failure Mechanisms at the Material Scale

The median IDA curves do not provide sufficient information about the mechanism of failure at the material scale. They just depict the global behaviour of the structures. To investigate this further, the steel and concrete material responses at the critical section of the columns (first integration point) are recorded during all the time-history analyses. At each time history analysis, the maximum compressive strain of core confined concrete is normalised to its crushing strain to obtain the normalised concrete strain ratio. In this way, all the calculated strain ratios become between zero and unity; where the unity corresponds to the onset of concrete crushing. On the other hand, the fatigue damage index of the outmost reinforcing bar at the same integration point is also recorded in all the IDAs.

In Fig. 13 and Fig. 14 the normalised concrete strains and fatigue damage indices are plotted against their corresponding maximum drift ratios. Fig. 13 shows the combined influence of cross-sectional shape, corrosion damage, and ground motion type on the failure modes of proposed uncorroded rectangular and circular RC columns at material scale. Based on the Figs. 13(a-b), while the failure mode of the uncorroded rectangular column is governed substantially by core concrete crushing when it is subjected to NFWP ground motions; the corresponding circular column, subject to the same suite of ground motions, fails by combined core concrete crushing and low-cycle fatigue failure of vertical reinforcement. However, Fig. 13(c) shows that under the NFNP ground motions, in several cases, low-cycle fatigue failure of vertical reinforcement followed by core concrete crushing (comparing to Fig. 13(a)) was the cause of failure. Furthermore, Fig. 13(d) shows that almost for all the individual NFNP ground motions, the core concrete crushing was preceded by the low-cycle fatigue failure. A similar trend can be seen in Fig. 13(f), where under the FF suite of ground motions the failure mode of the circular

column is mainly governed by low-cycle fatigue failure followed by core concrete crushing. This is because the outmost reinforcing bar (from the neutral axis) in the tension side of the circular section sustains large strains; and therefore, the low-cycle fatigue is its critical failure mode. However, similar to Fig. 13(a), under the FF ground motions, the failure of the uncorroded rectangular column is mainly governed by core concrete crushing.

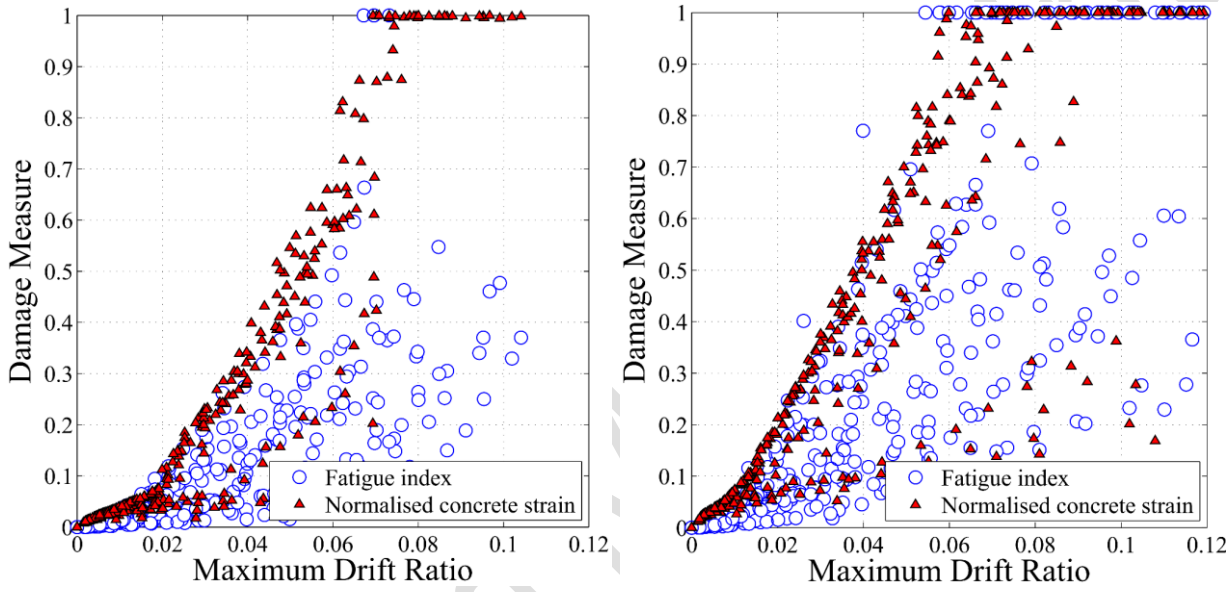

(a) **(b)**

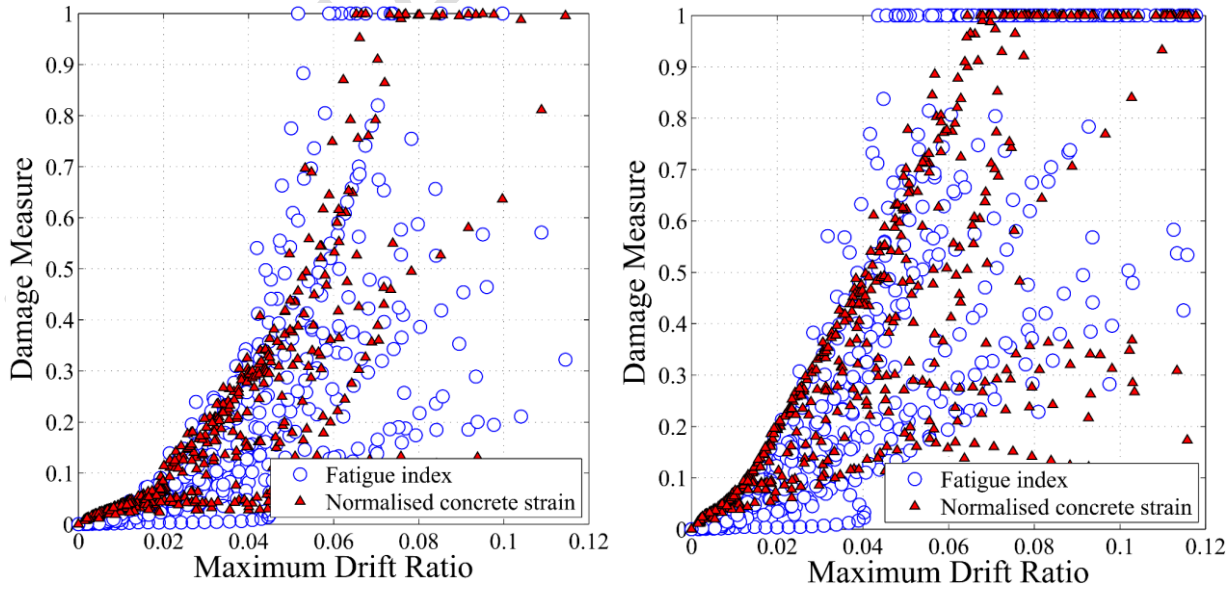

(c) **(d)**

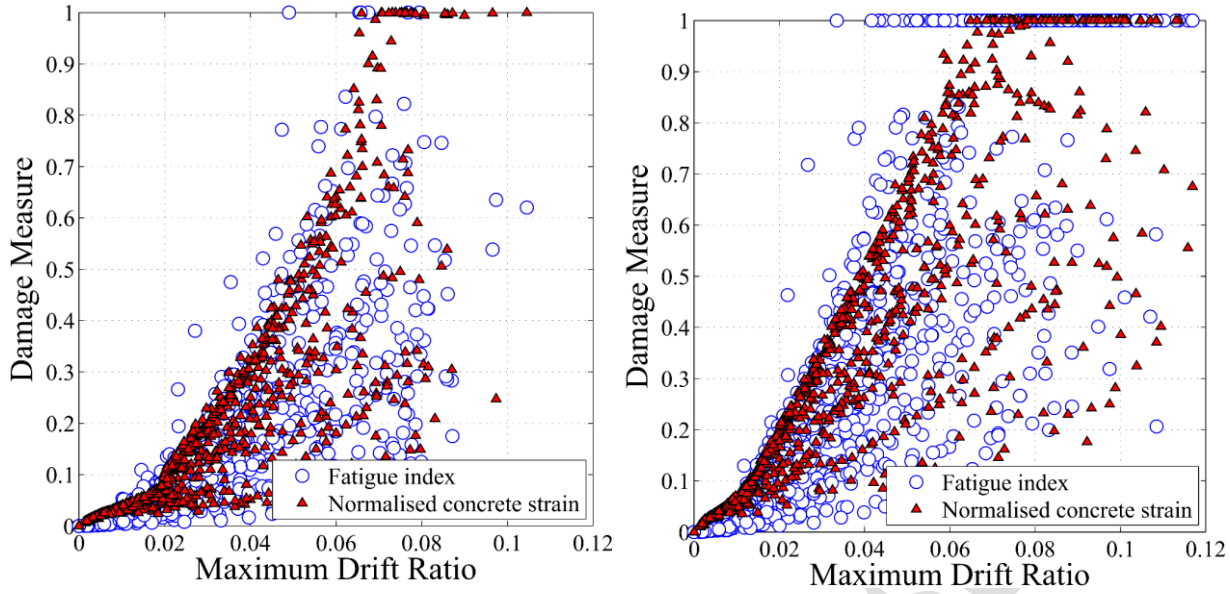

Fig. 13. Comparing failure mechanism of uncorroded columns subject to different ground motion sets: (a) NFWP, rectangular; (b) NFWP, circular; (c) NFNP, rectangular; (d) NFNP, circular; (e) FF, rectangular and (f) FF, circular.

Fig. 14 shows the effect of ground motion type and cross-sectional shape on 20% corroded columns. Based on Fig. 14, for all the ground motion suites, the core concrete crushing governs the failure mode of both columns with 20% mass losses. This is because the premature fracture of extremely corroded confining/tie reinforcement results in buckling of vertical reinforcement and crushing of core concrete. Therefore, it can be concluded that the proposed RC columns with severe corrosion damage experience more brittle failure mode under various types of ground motions.

It should be noted that the results of uncorroded and 20% corroded columns are shown in Fig. 13 and Fig. 14, respectively. The detailed results including 5% and 10% corroded columns are available in Figs. (S7-S12) of the attached "Supplementary Figures" file for each cross-sectional shape, ground motion type, and corrosion degree.

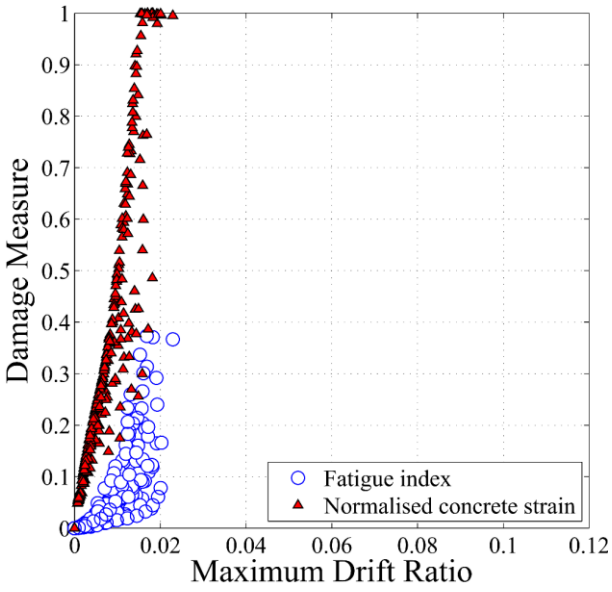

(a)

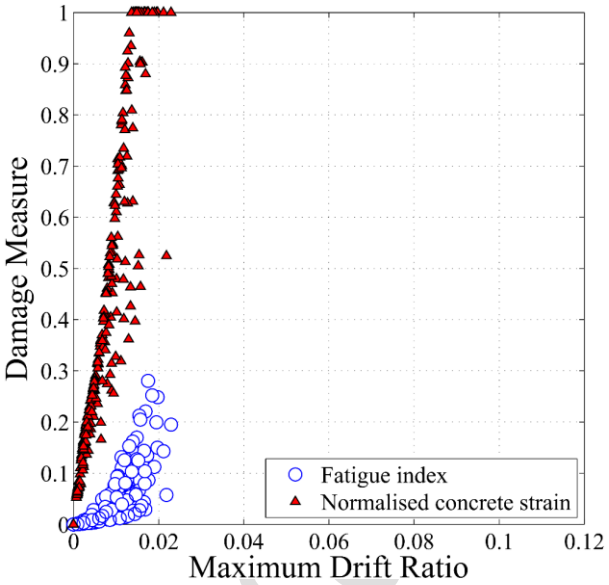

(b)

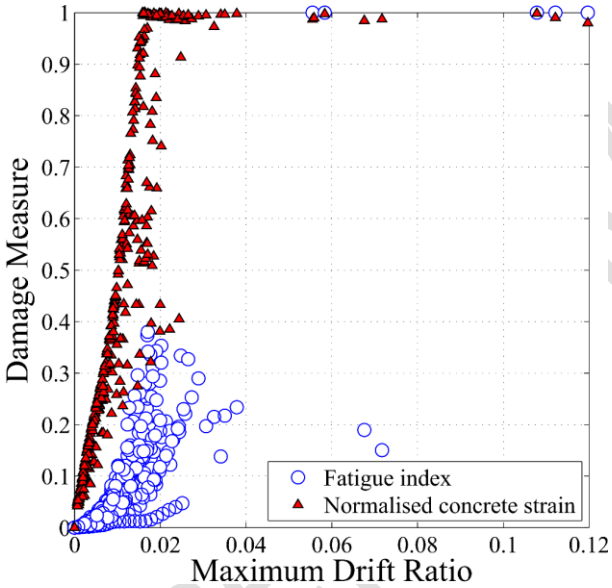

(c)

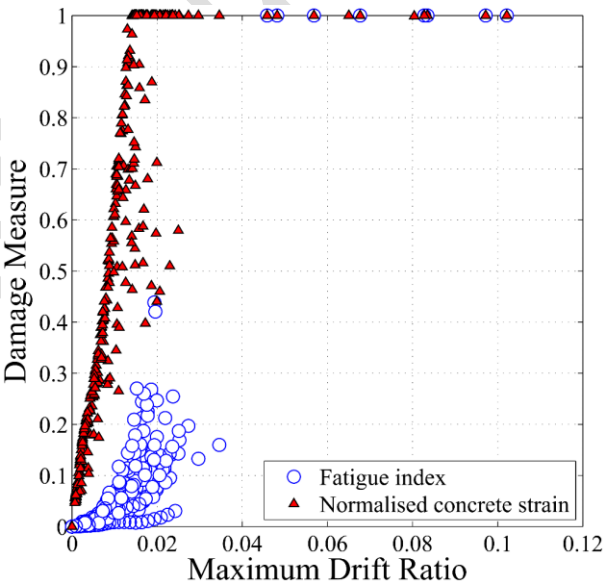

(d)

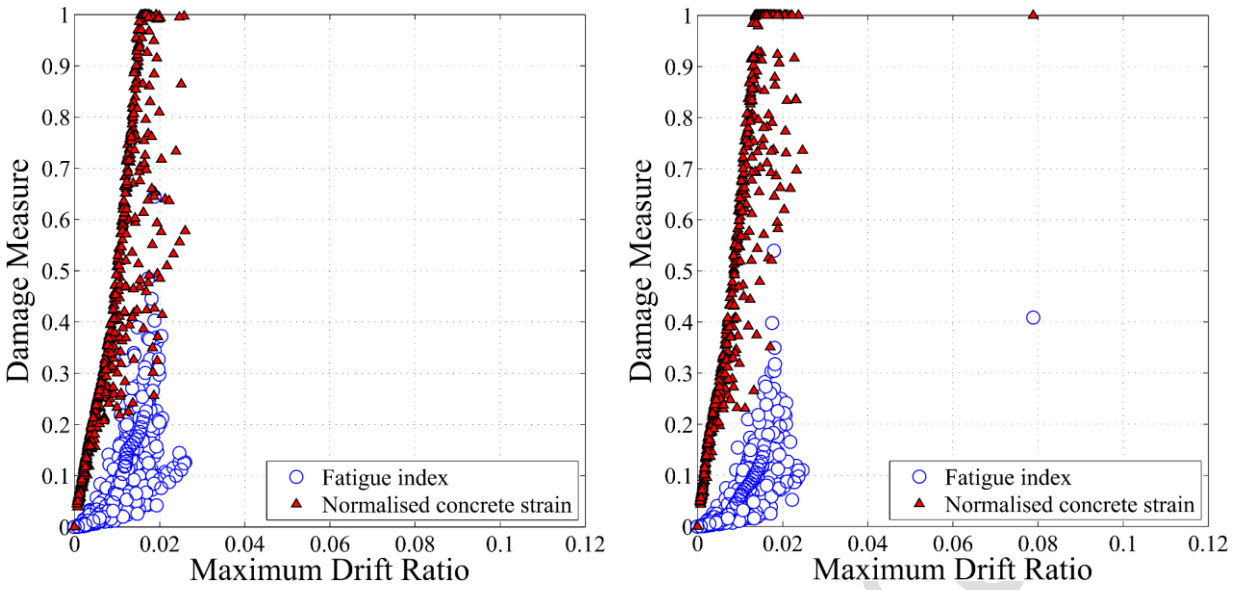

Fig. 14. Comparing failure mechanism of 20% corroded columns subject to different ground motion sets: (a) NFWP, rectangular; (b) NFWP, circular; (c) NFNP, rectangular; (d) NFNP, circular; (e) FF, rectangular and (f) FF, circular.

5. Seismic Fragility Analysis of the Proposed RC Bridge Piers

Seismic fragility curves are classical tools to evaluate the seismic vulnerability of structures. In these curves, the probability of exceeding a specific DLS is described as a conditional probability. To plot the fragility curves, first using the IDA results, the corresponding Maximum Drift Ratios (MDRs) of a given Intensity Measure (IM) are calculated for different ground motion records. Then, using the following fragility function the probability of exceeding a given DLS is calculated:

$$P\left(\mathrm{MDR} \geq \mathrm{DLS}_i \mid \mathrm{IM} = \mathrm{x}\right) = 1 - \Phi\left(\frac{\ln(\mathrm{DLS}_i) - \mu_{ln}}{\sigma_{ln}}\right) \quad (7)$$

where P(.) is the probability that MDR exceeds *i*th DLS given that IM=x and Φ(.) is the normal distribution function with a logarithmic mean of μ_{ln} (Eq. (8)) and logarithmic standard deviation of σ_{ln} (Eq. (9)):

$$\mu_{\ln} = \frac{1}{n}\sum_{i=1}^{n}\ln(\mathrm{MDR}_i) \quad (8)$$

$$\sigma_{\ln} = \frac{1}{n\text{-}1}\sqrt{\sum_{i=1}^{n}\left[\ln(\mathrm{MDR}_i) - \mu_{\ln}\right]^2} \quad (9)$$

where MDR_i is the value of MDR corresponding to IM=x for the *i*th ground motion record and *n* is the number of each ground motion record set. It should be noted that in this study $Sa(T_1)$ is considered as the IM.

To evaluate the combined influence of cross-sectional shape, mass loss, and ground motion type on the seismic vulnerability of RC bridge piers, the seismic fragility curves for both the rectangular and circular columns are developed in this part. The fragility curves are plotted for complete collapse DLS which is defined as the associated drift ratio of core concrete crushing as shown in Fig. 7. The effectiveness of considering corrosion damaged seismic DLSs is discussed in detail in Dizaj *et al*. [3].

Fig. 15 shows complete collapse fragility curves of the rectangular column for different mass losses and suites of ground motions. As it can be seen in Fig. 15, the fragility curve of NFWP ground motions is superior to the others. This shows that the probability of exceeding the complete collapse DLS is higher for the column subject to NFWP ground motions. For example, while for the FF ground motions the probability of exceeding complete collapse DLS is approximately 25% at $Sa\ (T_1) = 2g$; the corresponding probability for NFWP set is over 58 % (Fig. 15(a)) for the same IM. This is directly related to the trend of the IDA curves presented in Fig. 9(a), and the definition of seismic DLSs. Due to the impulsive damages of NFWP ground motions at the beginning of the shaking, the uncorroded rectangular column has failed in lower spectral accelerations at the complete collapse DLS (which is approximately 0.06 drift ratio according to Fig. 7(a)), comparing to those under NFNP and FF ground motions.

Moreover, for uncorroded and 5% corroded columns, up to $Sa(T_1) = 3g$ the fragility curve of FF set is below the others which indicates that in this range the rectangular column is less vulnerable under FF record set (Figs. 15(a-b)). Nonetheless, as mass loss increases the fragility curves of different ground

motion types become much closer. For example, for 20% corroded rectangular columns the probability of exceeding complete collapse DLS for different IMs is approximately the same for different ground motion sets.

Fig. 16 shows the complete collapse fragility curves of the circular column. Similar to the rectangular column, the circular column is much more vulnerable against NFWP record set in comparison with the NFNF and FF record sets. Moreover, the FF set has the least probability of exceeding complete collapse DLS for a specific IM. However, for the severe corrosion of reinforcing bars, the fragility curves are approximately overlapped.

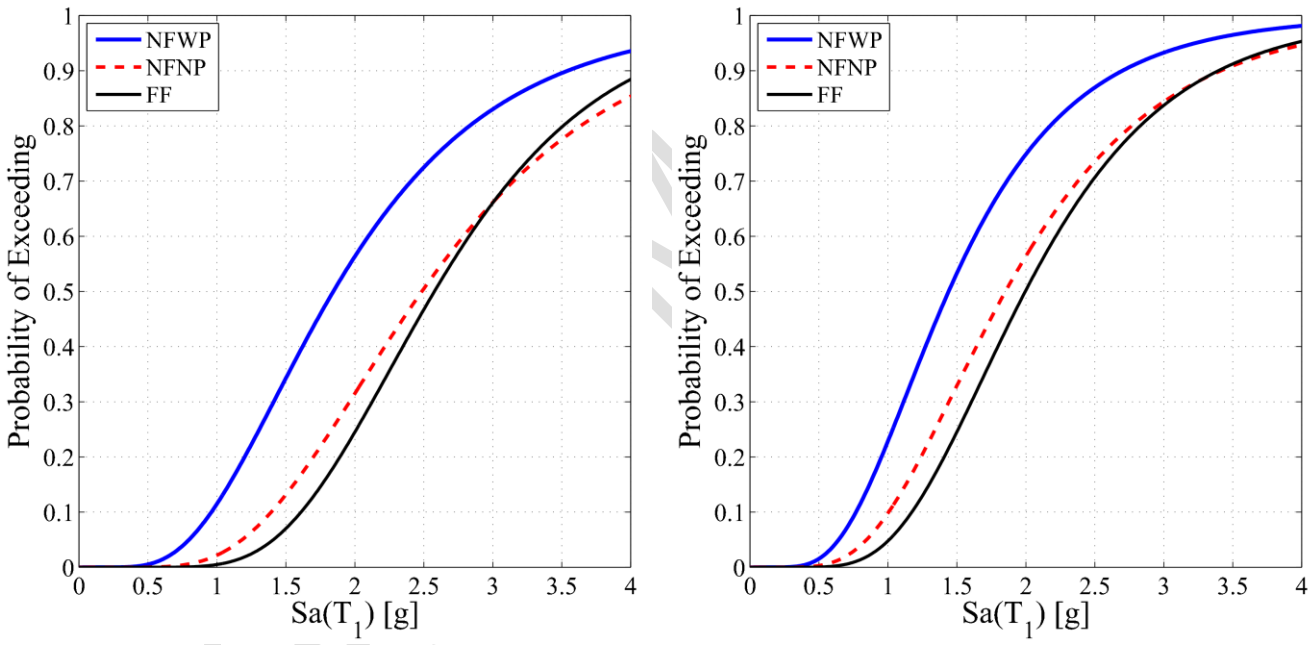

(a) **(b)**

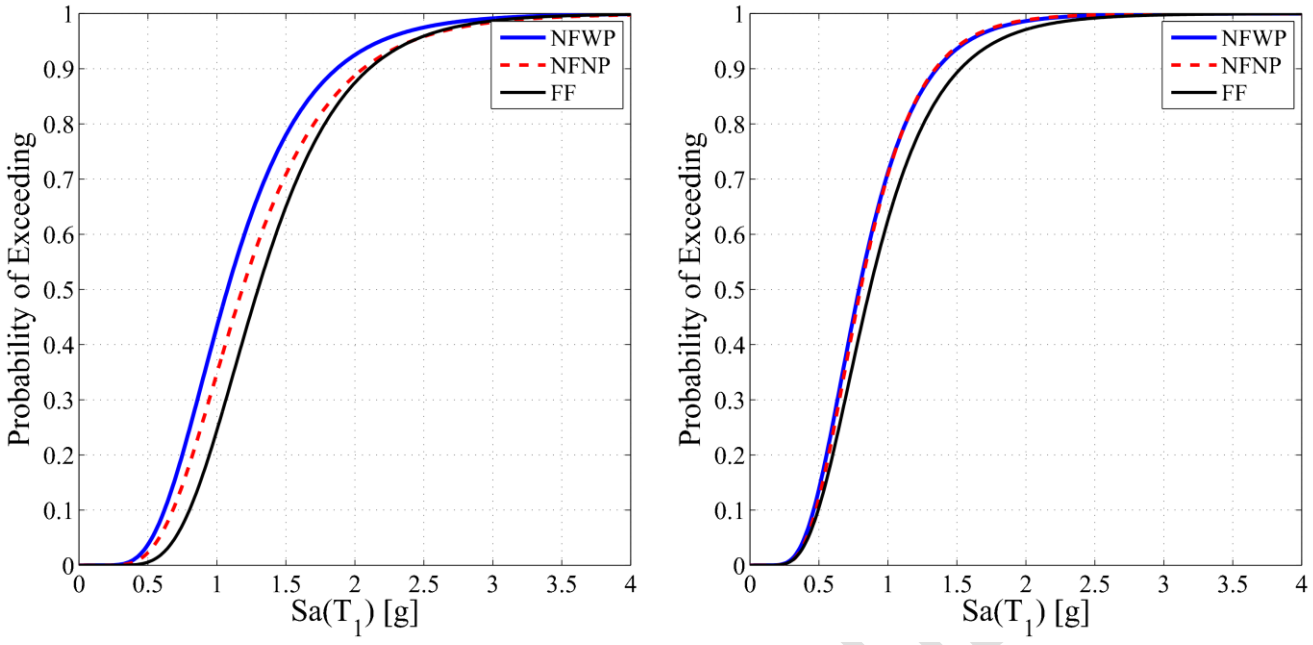

(c) (d)

Fig. 15. Complete collapse fragility curves for rectangular column: (a) uncorroded; (b) 5 % corroded; (c) 10% corroded and (d) 20% corroded

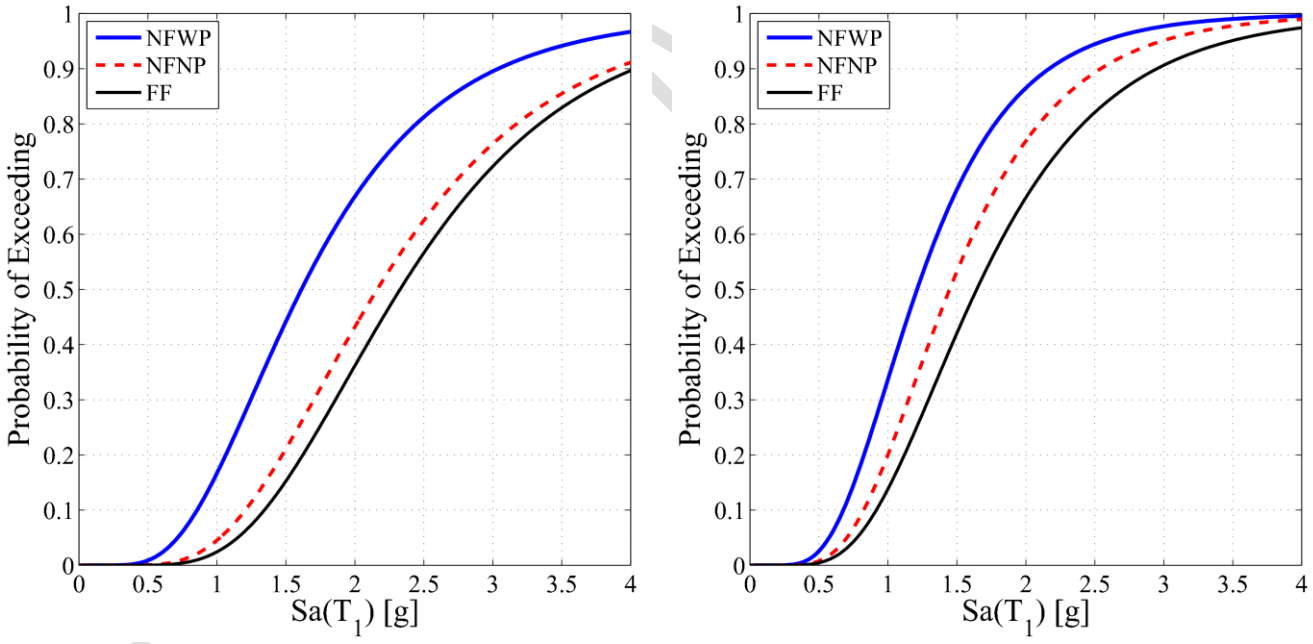

(a) **(b)**

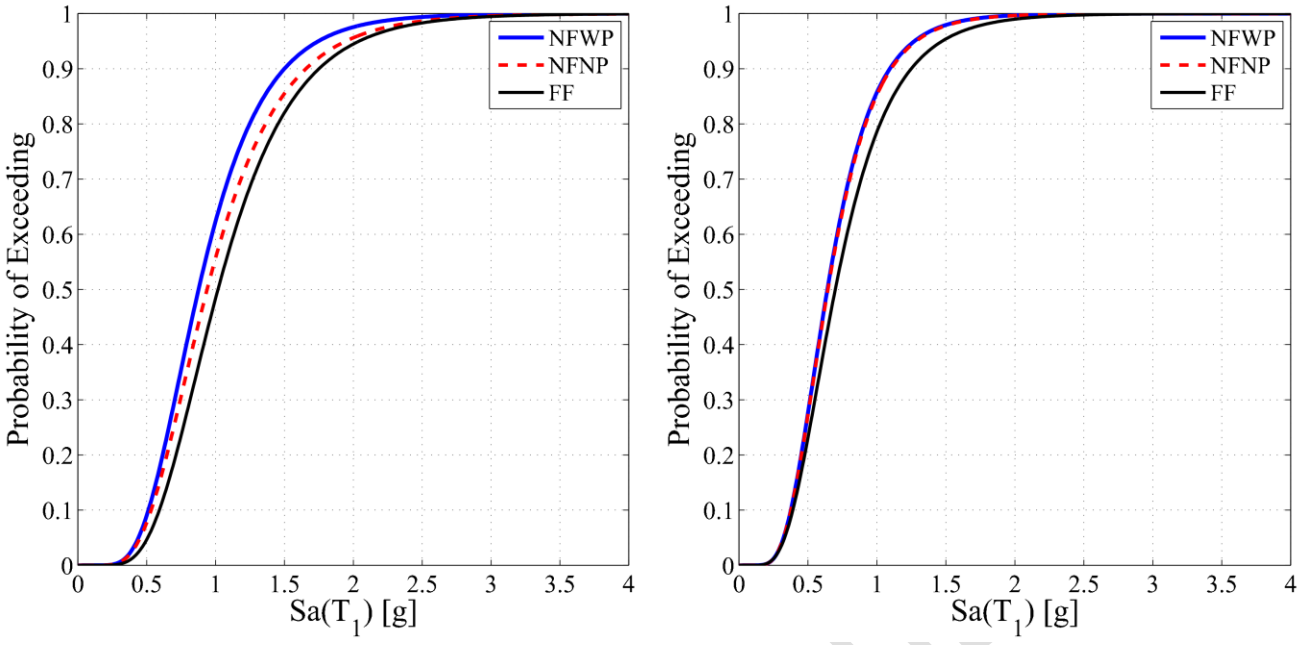

(c) **(d)**

Fig. 16. Complete collapse fragility curves for circular column: (a) uncorroded; (b) 5 % corroded; (c) 10% corroded and (d) 20% corroded

To investigate the impact of cross-sectional shape on the vulnerability of the proposed RC columns, in Fig. 17 the complete collapse fragility curves of the rectangular column for each suite of ground motion is compared with those of the circular column.

Fig. 17(a) shows that for each mass loss ratio, the fragility curve of the rectangular column is slightly below the corresponding curve of the circular column, and therefore, it is slightly less vulnerable than circular column under the NFWP ground motions (a similar trend is seen in Fig. 17(b)). However, based on Fig. 17(c), under the FF ground motions and scale factors greater than $Sa(T_1)$ = 3.5g, the probability of exceeding complete collapse DLS in the circular column is slightly less than the rectangular column for a specific $Sa(T_1)$. Furthermore, for scale factors greater than $Sa(T_1)$ = 1.5g the fragility curves of 10% corroded circular column is almost overlapped with 20% corroded rectangular column.

Based on the abovementioned discussion, it is concluded that for each mass loss ratio and each suite of ground motion, the circular column is slightly more vulnerable than its corresponding rectangular

column. However, it should be noted that in this study the complete collapse fragility curves are developed based on the associated crushing drift ratio of the outmost core concrete fibre, which is calculated using Eq. (1). The proposed empirical equations result is a lower value for circular columns in comparison to rectangular columns. Furthermore, considering the geometry of circular columns, it is a conservative assumption to consider the associated crushing of the outmost core concrete fibre as the complete collapse DLS. However, there are no explicit experimental studies in the literature to compare the failure mechanisms of the rectangular column with the circular column. This is an important area for future research.

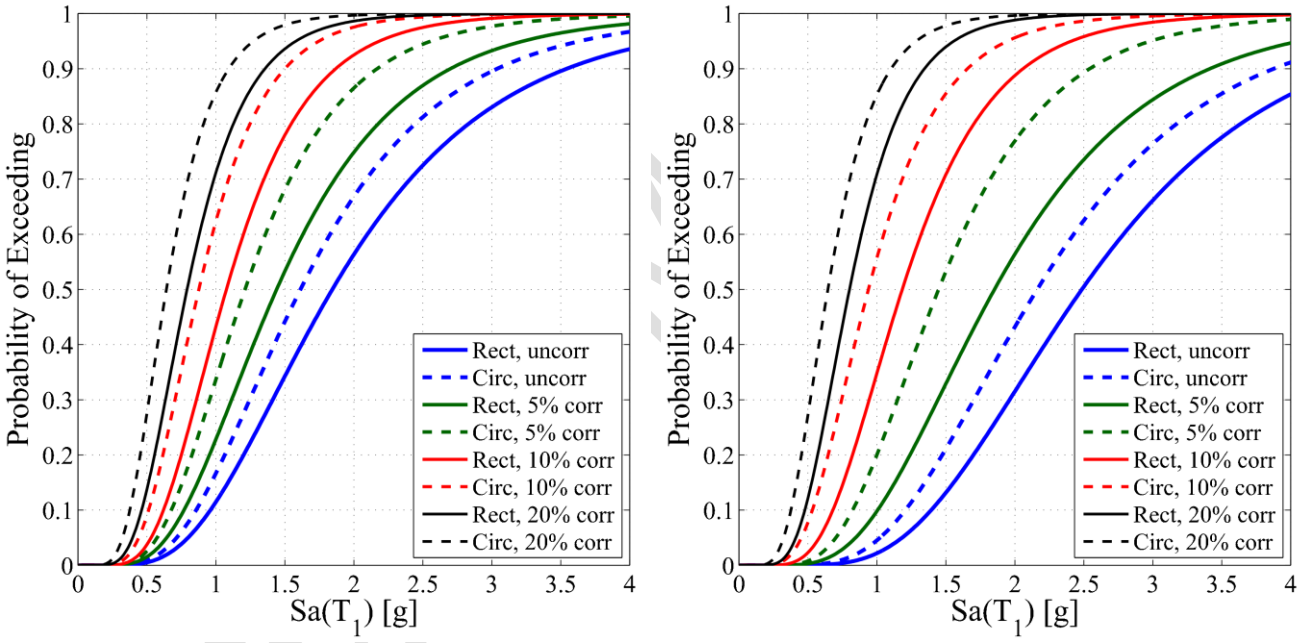

(a) **(b)**

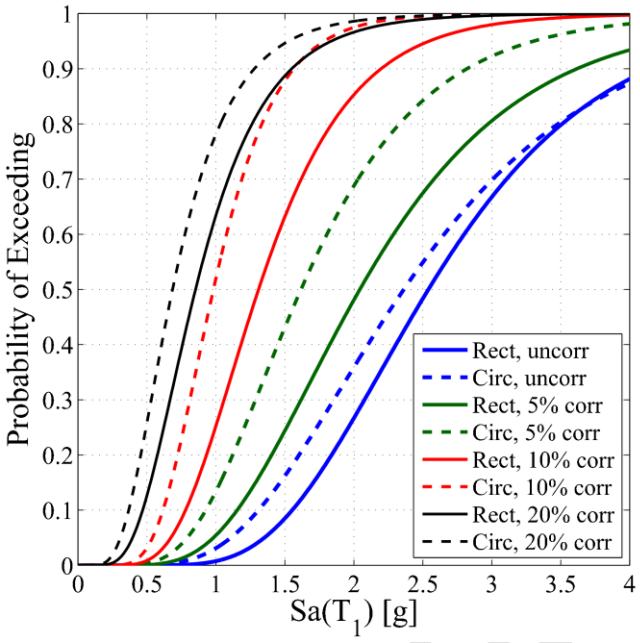

(c)

Fig. 17. Comparing complete collapse fragility curves of the considered RC columns subject to: (a) NFWP set; (b) NFNP set and (c) FF set

6. Pulse Effect and Influence of Non-Stationary Content of Ground Motion on Fragility of Proposed RC Bridge Piers

In this section, using Reweighted Volterra Series Algorithm (RVSA) (Alexander *et al.*, 2014), the impact of pulse in near-field ground motions on nonlinear dynamic response and fragility of the corroded columns is investigated. The RVSA matches the response spectrum of individual ground motion records to a target spectrum in such a way that the non-stationary characteristics of the original record such as overall shape, the timing of large pulses, variations in frequency content, and the nature of the ground motion (e.g., pulse-like or without pulse) remain unchanged. Moreover, the total time of an artificial ground motion record generated by the RVSA approach is the same as the original record. Further details about the RVSA and matching process are available in Alexander *et al*. (2014) and Kashani *et al*. (2017).

Employing RVSA, the spectral acceleration response of each NFWP and NFNP seed is matched to the median spectral acceleration response of NFNP ground motions to produce spectrally matched ground motions. The reason for selecting the median spectral acceleration response of NFNP ground motions as

the target spectrum is to investigate if the pulse component in the pulse-like ground motions has any significant impact on the nonlinear response of RC columns. Using the matched records, IDAs repeated for both the rectangular and circular columns with varied mass loss ratios. Fig. 18 shows a comparison between the original and matched ground motions of the Duzce earthquake record. Fig. 18 shows that the timing of large pulses, as well as the overall shape of the envelope, are not affected by the matching process. In Fig. 19, the spectral acceleration response of both the original and matched NFWP set is plotted against the median spectrum of the NFNP set. Fig. 19(b) shows that the spectral acceleration response of all the matched ground motions is approximately the same.

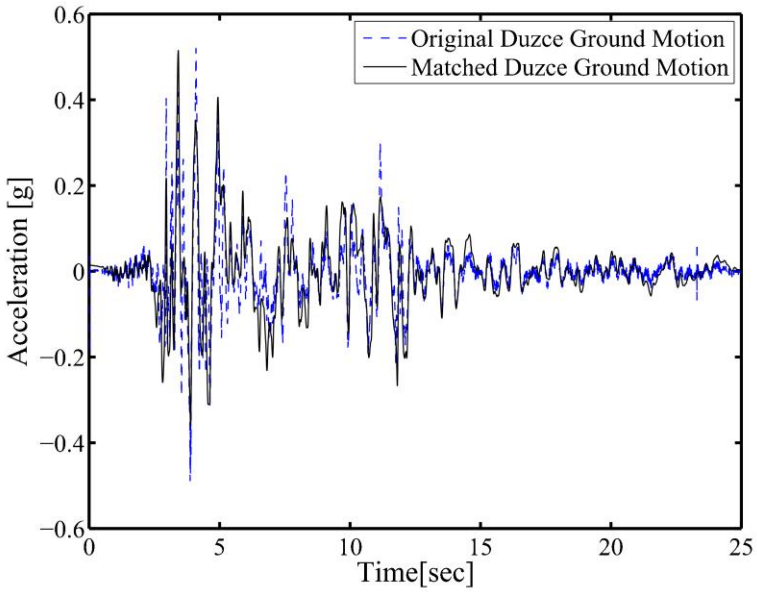

Fig. 18. Comparing matched and original envelope of Duzce earthquake

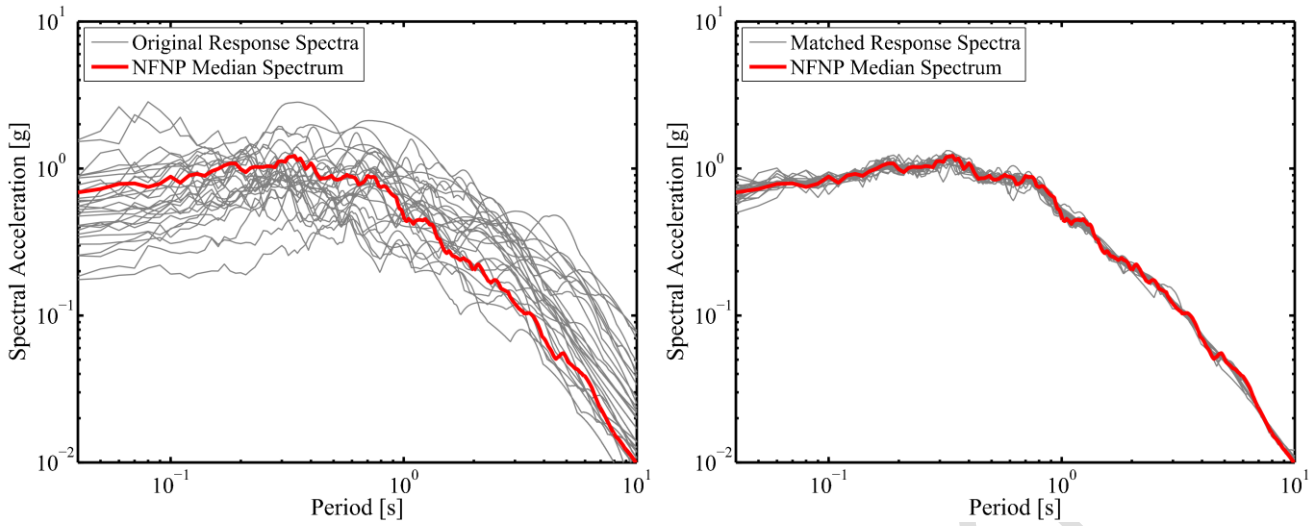

(a) **(b)**

Fig. 19. Response spectra of NFWP set versus NFNP median spectrum: (a) original seeds; (b) matched seeds

Fig. 20 compares the median IDA results of matched ground motions with those of original ones. As it is shown in Fig. 20, while under the original NFWP ground motions the median IDA response of both the rectangular and circular columns with varied mass loss ratios are significantly lower than those of NFNP, they are approximately identical under the matched near-field ground motions. However, Fig. 20(b) shows that the median IDA response of rectangular column with varied mass loss ratios under the matched NFWP ground motions is slightly less than those subjected to matched NFNP suite. This shows that the effect of pulses on the global nonlinear dynamic behaviour of a single column is negligible. Similar behaviour can be seen in Fig. 20(d). For instance, the median IDA curve of 20% corroded circular column subject to NFWP coincides with that of NFNP.

In Fig. 21, complete collapse fragility curves of the considered columns subjected to matched near-field ground motions are plotted. Fig. 21 indicates that both the rectangular and circular columns under matched NFWP ground motions are slightly more fragile than those subjected to matched NFNP. Therefore, the effect of pulse on the probability of failure of the columns is almost negligible.

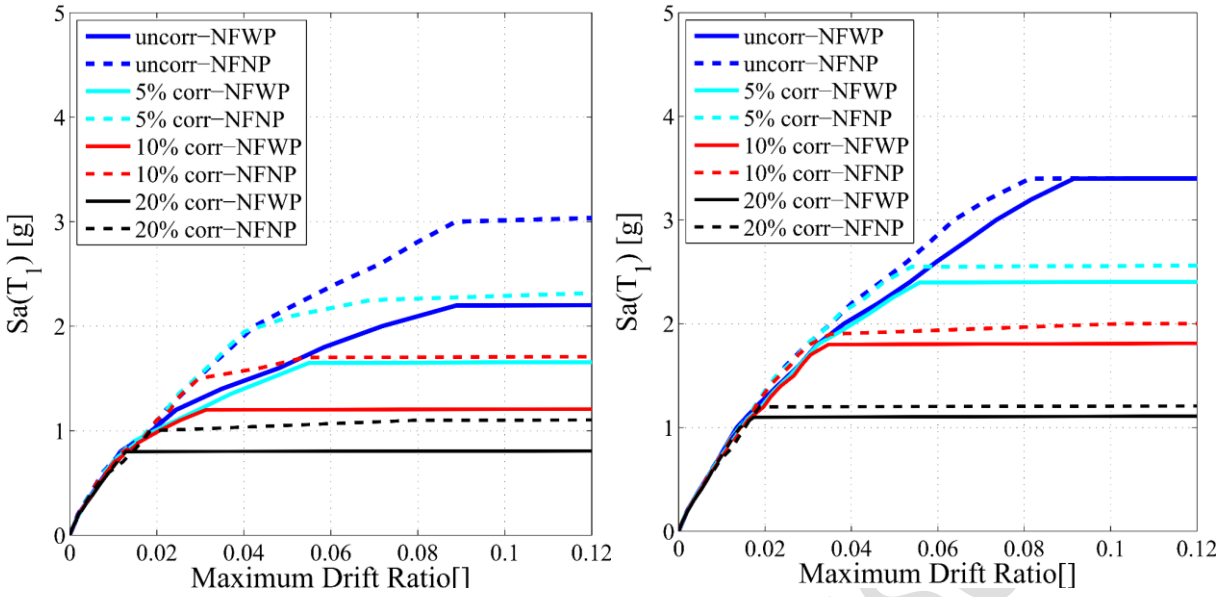

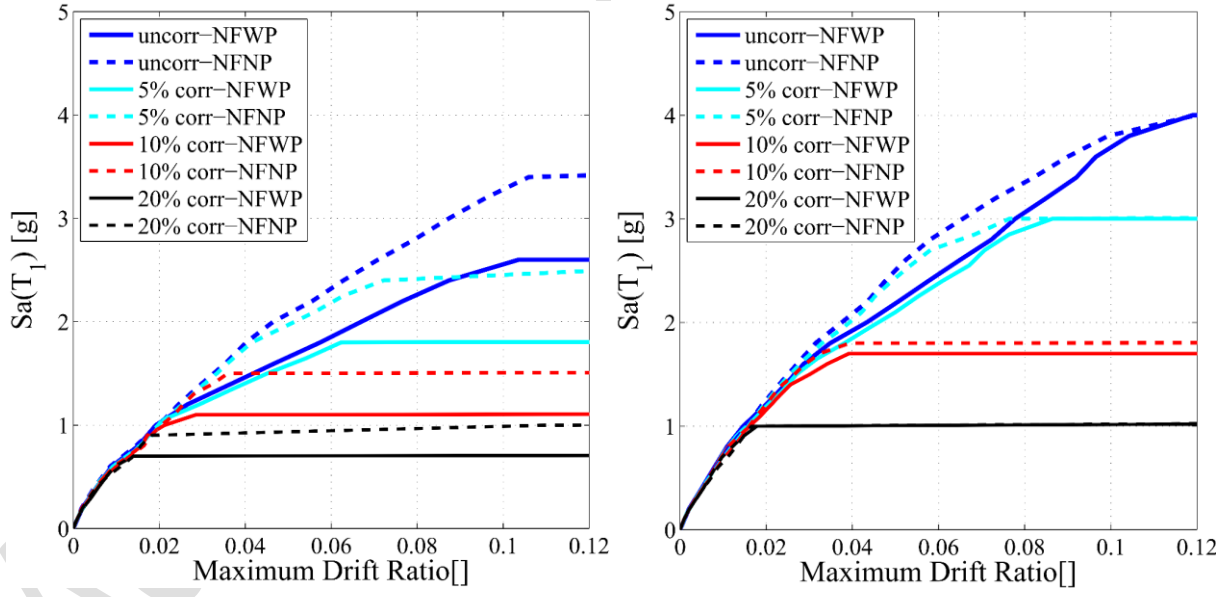

Fig. 20. Median IDA curves for original and matched near-field ground motion sets: (a) rectangular, original; (b) rectangular, matched; (c) circular, original; (d) circular, matched

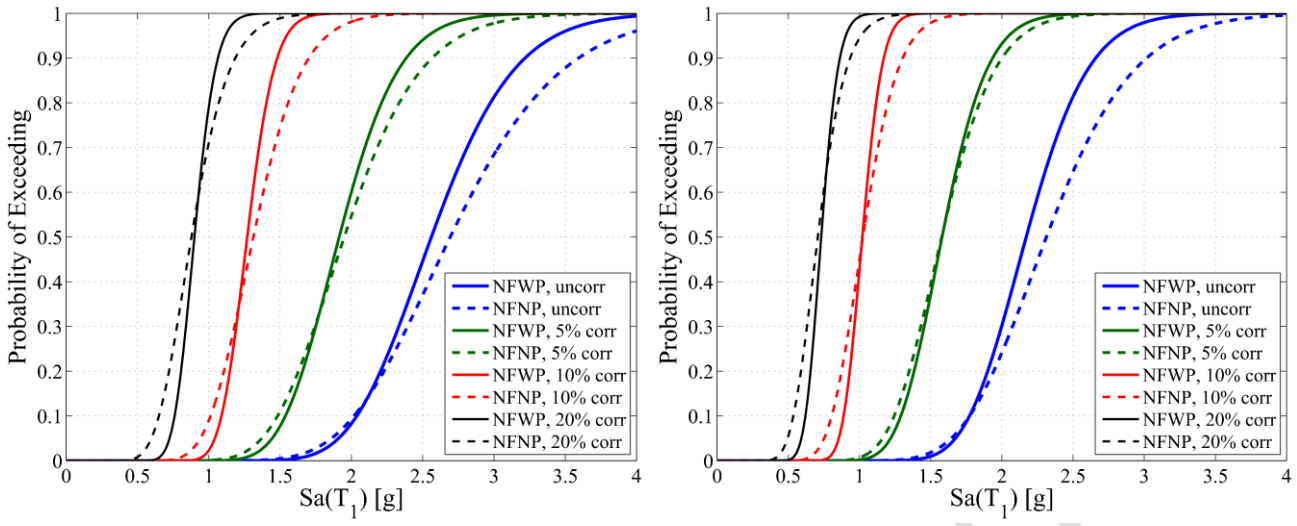

Fig. 21. Complete collapse fragility curves for matched NFWP and NFNP records: (a) rectangular column; (b) circular column

7. Conclusions

The combined influence of corrosion damage, cross-sectional shape and ground motion type on the nonlinear dynamic response, failure mechanism and seismic fragility of RC bridge piers was investigated. To this end, a rectangular and a circular cross-section column with four mass loss ratios such as, 0%, 5%, 10% and 20%, and three different suites of ground motions, such as FF, NFWP, and NFNP were considered for the nonlinear analyses (static and dynamic). Using the corrosion-dependent DLSs, fragility curves were plotted for each column and ground motion type. Finally, employing RVSA, the pulse effect on the nonlinear dynamic behaviour of corrosion damaged RC columns was explored. The important findings of this study are summarised as follows:

- The key conclusions for the effect of cross-sectional shape:

  The circular column, with uncorroded and 5% corroded reinforcing bars fails in a relatively greater intensity level of input earthquake record in comparison to its corresponding rectangular

column. The reason could be attributed to the more efficient confinement action in the circular section which results in a more gradual failure of core concrete under uniaxial loading. However, for columns with 10% and 20% corroded reinforcing bars, the insufficient confinement level due to the premature fracture of highly corroded transverse reinforcement causes more brittle failure mode; and therefore, the median IDA response of both columns for these extreme corrosion scenarios become almost identical.

The rectangular column, for a given percentage of mass loss and ground motion type, is slightly less fragile than its corresponding circular column. For example, while the probability of failure of 10 % corroded circular column under NFWP ground motion suite is approximately 90%; the failure probability of the corresponding rectangular column is around 80%. This could be due to the adopted seismic DLSs. The failure of the columns is core concrete crushing which is obtained based on an empirical equation. This equation gives a smaller value for the circular section. Further research is required in this area in the future.

Ground motion type significantly affects the damage sequence and failure mode of the uncorroded rectangular columns. However, the damage sequence in the uncorroded circular column is mainly the core concrete crushing preceded by low-cycle fatigue failure of vertical reinforcements.

- The key conclusions for the effect of ground motion type:

Under NFWP ground motions, the first mode spectral acceleration response of the proposed uncorroded and 5% corroded columns, corresponding to the collapse threshold, is significantly smaller than the other two types. This is because the NFWP ground motions impose impulsive damage to the columns during the first big pulse, and hence, the damaged columns do not respond to the following cycles. Therefore, under the NFWP ground motions, the probability of exceeding a specific intensity measure is significantly higher for both columns uncorroded and 5% corroded

columns. However, for the higher corrosion levels, due to the brittle failure mode, both columns fail at approximately the same earthquake intensity level regardless of ground motion type.

Under the matched NFWP ground motions, both the rectangular and circular columns are slightly more fragile than those subjected to matched NFNP ground motions. For example, while under the NFNP ground motions the probability of failure of 5% corroded reinforcement is approximately 95%; the failure probability of the same column under the matched NFWP ground motions is about 90%. This shows that the pulses do not have a significant influence on the fragility of the proposed columns. However, this requires further investigation on a variety of structures, and a large number of pulse-like ground motions. This is an area for future research.

- The key conclusions for the effect of corrosion damage:

As corrosion damage increases, both columns fail at approximately the same first mode spectral acceleration. For severe corrosion damage (20% of mass loss), the median IDA response of the columns under any type of the considered ground motions becomes much closer to each other. Moreover, severe corrosion damage results in the brittle failure mode of both the proposed columns under all types of the considered ground motions. This is because of the buckling of vertical reinforcement and crushing of core concrete due to premature fracture of corroded confinement reinforcement. Moreover, severely corroded columns have approximately the same probability of failure for a given spectral acceleration.

Declarations

Funding: Not applicable.

Conflicts of interest/Competing interests:

- All authors have participated in (a) conception and design, or analysis and interpretation of the data; (b) drafting the article or revising it critically for important intellectual content; and (c) approval of the final version.

- This manuscript has not been submitted to, nor is under review at, another journal or other publishing venue.

- The authors have no affiliation with any organization with a direct or indirect financial interest in the subject matter discussed in the manuscript

Availability of data and material: Not applicable.

Code availability: Not applicable.

Authors' contributions:

Ebrahim Afsar Dizaj: Conceptualization, Formal analysis, Methodology, Finite Element modelling, Writing original draft. **Mohammad Mehdi Kashani**: Supervision, Validation, Methodology, Review & Editing.

References

Alexander, N.A., Chanerly, A.A., Crew, A.J., Bhattacharaya, S. (2014). Obtaining spectrum matching time series using a Reweighted Volterra Series Algorithm (RVSA). *Bulletin of the Seismological Society of America* 104(4):1663-1673.

Alipour, A., Shafei, B., Shinozuka, M. (2011). Performance evaluation of deteriorating highway bridges located in high seismic areas. *Journal of Bridge Engineering* 6: 597-611.

ASCE. 2013. Report card for America's Infrastructure. ⟨http://www.infrastructurereportcard.org/bridges/⟩.

Billah, A.H.M.M., Alam, M.S. (2018). Seismic performance evaluation of multi-column bridge bents retrofitted with different alternatives using incremental dynamic analysis. *Engineering Structures*, 165: 441-456.

Bagheri, M., Hosseini, S.A., Keshtegar, B., Correira, A.F.O, Trung, N.T. (2020). Uncertain time-dependent reliability analysis of corroded RC structures applying three-term conjugate method, Engineering Failure Analysis, 115: 104599. https://doi.org/10.1016/j.engfailanal.2020.104599.

Biondini, F., Frangopol, D.M. (2009). Lifetime reliability-based optimization of reinforced concrete cross-sections under corrosion. *Structural Safety* 31:483–489.

Biondini, F., Camnasio, E., Titi, A. (2015). Seismic resilience of concrete structures under corrosion. *Earthquake Engineering and Structural Dynamics*, 2015, 44:2445–2466.

Camnasio, E. (2013). Lifetime performance and seismic resilience of concrete structures exposed to corrosion. Ph.D thesis, Polytechnic University of Milan, Italy.

Choe, D.E., Gardoni, P., Rosowsky, D., Haukaas, T. (2008). "Probabilistic capacity models and seismic fragility estimates for RC columns subject to corrosion." Reliab. Eng. Syst. Saf. 93 (3): 383–393. https://doi.org/10.1016/j.ress.2006.12.015.

Choe, D.E., Gardoni, P., Rosowsky, D., Haukaas, T. (2009). Seismic fragility estimates for reinforced concrete bridges subject to corrosion. *Structural Safety* 31(4): 275-283.

Coronelli, D., Gambarova, P. (2004). Structural assessment of corroded reinforced concrete beams: modeling guidelines. *Journal of Structural Engineering* 130(8): 1214-1224.

Cui, F., Zhang, H., Ghosn, M., and Xu, Y. (2018). Seismic fragility analysis of deteriorating RC bridge substructures subject to marine chloride-induced corrosion. *Engineering Structures* 155: 61-72.

Deng, P., Zhang, C., Pei, S., Jin, Z. (2018). Modeling the impact of corrosion on seismic performance of multi-span simply-supported bridges. *Construction and Building Materials* 185: 193-205.

Dhakal, R.P., Maekawa, K. (2002). Reinforcement stability and fracture of cover concrete in reinforced concrete members. *Journal of Structural Engineering* 128(10): 1253-1262.

Dizaj, E.A., Madandoust, R., Kashani, M.M. (2018a). Probabilistic Seismic Vulnerability Analysis of Corroded Reinforced Concrete Frames Including Spatial Variability of Pitting Corrosion. *Soil Dynamics and Earthquake Engineering* 114: 97-112.

Dizaj, E.A., Madandoust, R., Kashani, M.M. (2018b). Exploring the impact of chloride-induced corrosion on seismic damage limit states and residual capacity of reinforced concrete structures. *Structure and Infrastructure Engineering* 14(6): 714-729.

Du, Y. G., Clark, L. A., Chan, A. H. C. (2005a). Residual capacity of corroded reinforcing bars. *Magazine of Conc Res*. 57 (3): 135–147.

Du, Y. G., Clark, L. A., Chan, A. H. C. (2005b). Effect of corrosion on ductility of reinforcing bars. *Magazine of Conc Res*. 57 (7): 407–419.

Faroz, S.A., Pujari, N. N., Ghosh, S. (2016). Reliability of a corroded RC beam based on Bayesian updating of the corrosion model. *Engineering Structures* 126:457–468.

FEMA P695. (2009). Quantification of Building Seismic Performance Factors. Federal Emergency Management Agency, Washington, DC.

Firouzi, Afshin., Abdolhosseini, Mohaddeseh., Ayazian, Rouhollah. (2020). Service life prediction of corrosion-affected reinforced concrete columns based on time-dependent reliability analysis. Engineering Failure Analysis, 117, 104944. https://doi.org/10.1016/j.engfailanal.2020.104944.

Gaal, G.C.M. (2004). Prediction of deterioration of concrete bridges. PhD thesis, TU Delft.

Ge X, Dietz MS, Alexander NA. *et al.* (2020). Nonlinear dynamic behaviour of severely corroded reinforced concrete columns: shaking table study. *Bull Earthquake Eng*, 18: 1417–1443. https://doi.org/10.1007/s10518-019-00749-3.

Ghosh, J., Padgett, J. E. (2010). Aging considerations in the development of time-dependent seismic fragility curves. *Journal of Structural Engineering* 136(12): 1497-1511.

Ghosh, J., Sood, P. (2016). Consideration of Time-Evolving Capacity Distributions and Improved Degradation Models for Seismic Fragility Assessment of Aging Highway Bridges. *Reliability Engineering & System Safety* 154:197–218.

Gu, X., Guo, H., Zhou, B., Zhang, W., Jiang, C. (2018). Corrosion non-uniformity of steel bars and reliability of corroded RC beams. *Engineering Structures* 167:188–202.

Guo, A., Yuan, W., Lan, Ch., Guan, X. and Li, H. (2015). Time-dependent seismic demand and fragility of deteriorating bridges for their residual service life. *Bull Earthq Eng* 13 (8): 2389-2409. DOI 10.1007/s10518-014-9722-x

HAZUS-MH MR5. (2010). Earthquake loss estimation methodology. Technical and User's Manual. Department of Homeland Security, Federal Emergency Management Agency, Mitigation Division. Washington D.C.

Imperatore, S., Rinaldi, Z., Drago, C. (2017). Degradation relationships for the mechanical properties of corroded steel rebars. *Construction and Building Materials* 148: 219–230.

Kashani MM, Ge X, Dietz MS, Crewe AJ, Alexander NA. (2019b). Significance of non-stationary characteristics of ground-motion on structural damage: shaking table study. Bulletin of Earthquake Engineering, 17(9): 4885-4907. https://doi.org/10.1007/s10518-019-00668-3.

Kashani, M. M., Lowes, L.N., Crewe, A.J., Alexander, N.A. (2016). Nonlinear fibre element modelling of RC bridge piers considering inelastic buckling of reinforcement. *Eng Struct* 116: 163-177.

Kashani, M.M., Barmi, AK., Malinova, S. (2015a). Influence of inelastic buckling on low-cycle fatigue degradation of reinforcing bars. Construction and Building Materials. 94: 644-655.

Kashani, M.M., Lowes, L., Crewe, A.J., Alexander, N.A. (2015b). Phenomenological hysteretic model for corroded reinforcing bars including inelastic buckling and low-cycle fatigue degradation. *Computers and Structures* 156: 58-71.

Kashani, M. M., Maddocks, J., Afsar Dizaj, E. (2019a). Residual Capacity of Corroded Reinforced Concrete Bridge Components: A State-of-the-Art Review. *Journal of Bridge Engineering* 24 (7), 03119001.

Kashani, M. M., Málaga-Chuquitaype, C., Yang, S., and Alexander, N.A. (2017). Influence of non-stationary content of ground-motions on nonlinear dynamic response of RC bridge piers. *Bulletin of Earthquake Engineering* 15(9): 3897-39

Kashani, M.M., Salami, M.R., Goda, K., Alexander, N. (2018). Nonlinear flexural behaviour of RC columns including bar buckling and fatigue degradation. *Magazine of Concrete Research* 70(5): 231-247.

Lehman, D. E. and J. P. Moehle. (2000). Seismic Performance of Well-Confined Concrete Bridge Columns. PEER 1998/01, Pacific Earthquake Engineering Research Center, Berkeley, CA.

Li, C., Hao, H., Li, H., Bi, K. (2015). Seismic Fragility Analysis of Reinforced Concrete Bridges with Chloride Induced Corrosion Subjected to Spatially Varying Ground Motions. *International Journal of Structural Stability and Dynamics* 6:1-27.

Lu, Y., Hajirasouliha, I., Marshall, A.M. (2018). Direct displacement-based seismic design of flexible-base structures subjected to pulse-like ground motions. *Engineering Structures* 168: 276–289.

Mander, J.B., Priestley, M.J.N., Park, R.J. (1988). Theoretical stress–strain model for confined concrete. *Journal of Structural Engineering* 114(8):1804–25.

Manson SS. 1965. “Fatigue: A complex subject-Some simple approximations.” Exp Mech. 5 (7): 193–226.

Meda, A., Mostosi, A., Rinaldi, Z., Riva, P. (2016). Corroded RC columns repair and strengthening with high performance fiber reinforced concrete jacket. *Materials and Structures* 49 (5), 1967-1978.

McKenna, F. (2011). OpenSees: a framework for earthquake engineering simulation. Computing in Science & Engineering 13(4): 58-66.

Ni Choine, M., Kashani, M. M., Lowes, L.N., O'Connor, A., Crewe, A.J., Alexander, N.A. (2016). Nonlinear dynamic analysis and seismic fragility assessment of a corrosion damaged integral bridge. *International Journal of Structural Integrity* 7(2): 227-239.

Pu, W., Wu, M., Huang, B., Zhang, H. (2018). Quantification of response spectra of pulse-like near-fault ground motions. *Soil Dynamic and Earthquake Engineering* 104:117–130.

Rajput, A.S., Sharma, U.K., Engineer, K. (2019). Seismic retrofitting of corroded RC columns using advanced composite materials, *Engineering Structures* 181: 35-46.

Rao, A.S., Lepech, M.D., Kiremidjian, A. (2017). Development of time-dependent fragility functions for deteriorating reinforced concrete bridge piers. *Structure and Infrastructure Engineering* 13(1):67-83. https://doi.org/10.1080/15732479.2016.1198401

Salami, M.R. (2016). Seismic Performance of Buildings Considering Mainshock-Aftershocks: Improvement in Record Selection and Advanced Nonlinear Fibre Beam-Column Model for RC Framed Structures. PhD Thesis, University of Bristol.

Scott, B., Park, R., Priestley, M. (1982). Stress-strain behavior of concrete confined by overlapping hoops at low and high strain rates. *ACI Journal* 79(1): 13-27.

Priestley, M., Paulay, T. (1992). Seismic design of reinforced concrete and masonry buildings. New York: *John Wiley & Sons*, Inc.

Sun, B., Xiao, R.C., Ruan, W.D., Wang, P.B. (2020). Corrosion-induced cracking fragility of RC bridge with improved concrete carbonation and steel reinforcement corrosion models. Engineering Structures, 208, 110313. https://doi.org/10.1016/j.engstruct.2020.110313.

Titi, A., Biondini, F., Frangopol, D.M. (2014). Lifetime resilience of aging concrete bridges under corrosion. *The 7th International Conference on Bridge Maintenance, Safety and Management, IABMAS*.
Vamvatsikos, D., Cornell, C.A. (2002). Incremental dynamic analysis. *Earthquake Engineering and Structural Dynamics*, 31(3): 491-514.

Vecchi, F., Belletti, B. (2021). Capacity assessment of existing RC columns. Buildings 11(4), 161, https://doi.org/10.1680/jbren.20.00044.

Wallbank, E.J. (1989). The performance of concrete in bridges: A survey of 200 highway bridges, London.

Xu, J.G., Wu, G., Feng, D.C., Cotsovos, D.M., Lu, Y. (2020). Seismic fragility analysis of shear-critical concrete columns considering corrosion induced deterioration effects. Soil Dynamics and Earthquake Engineering, 134, 106165. https://doi.org/10.1016/j.soildyn.2020.106165.

Yalciner, H., Sensoy, S., Eren, O. (2012). Time-dependent seismic performance assessment of a single-degree-of-freedom frame subject to corrosion, Engineering Failure Analysis, 19:109-122. https://doi.org/10.1016/j.engfailanal.2011.09.010.

Yuan, W., Guo, A., Li, H. (2017). Seismic failure mode of coastal bridge piers considering the effects of corrosion-induced damage. *Soil Dynamics and Earthquake Engineering* 93:135-146.

Zhang, M., Song, H., Lim, S., Akiyama, M., Frangopol, D.M. (2019). Reliability estimation of corroded RC structures based on spatial variability using experimental evidence, probabilistic analysis and finite element method. Engineering Structurs, 192: 30-52. https://doi.org/10.1016/j.engstruct.2019.04.085.

Zhao, J., Sritharan, S. Modeling of strain penetration effects in fiber-based analysis of reinforced concrete structures. *ACI structural journal* 104(2): 133-141.